

Article

# Oxidative Dehydrogenation of Liquefied Petroleum Gas on Copper, Zinc and Iron Oxide Impregnated on MFI Zeolite Assisted by Electric Power

Amin Alamdari and Ramin Karimzadeh \*

Department of Chemical Engineering, Tarbiat Modares University (TMU), Jalal Al Ahmad Highway, P.O. Box, Tehran 14115-4838, Iran; amin.alamdari@modares.ac.ir

\* Correspondence: ramin@modares.ac.ir; Tel.: +98-21-8288-3315

Received: 26 May 2018; Accepted: 22 June 2018; Published: 30 June 2018



**Abstract:** Olefin was produced with a non-conventional method using an electric field exerted on zeolites. The lattice oxygen mobility increases with a decrease in band gap, leading to an increase in olefin yield. By impregnating the transition metal, an increase in carrier concentration occurs. The external electric field changes the Fermi level. In this research, HZSM-5 was placed in an external DC electric field with strength appropriate for studying its catalytic performance. The Fermi level changed with the metal type and the external electric field. The increase in permittivity with temperature extracts higher energy from the external electric field. In catalytic reactions assisted by the external DC electric field, at 510 °C, the yield was approximately equal to the yield in a conventional reaction at 650 °C. With regard to TGA, in the catalytic reaction assisted by the external DC electric field, the produced coke declined. The results showed that the maximum yield value (50.54%) and conversion (92.81%) were obtained at 650 °C with an input electrical current of 12 mA, a gap distance of 10 mm and a metal loading of 4 wt. % over FeHZSM-5.

**Keywords:** catalytic activity; transition metal oxide; Fermi surface; electrical properties; MFI zeolite

## 1. Introduction

Ethylene and propylene are raw materials used in the production of plastic materials, synthetic polymers, and a varied range of chemicals [1,2]. Demand for ethylene production is rapidly increasing. In China, ethylene production was 10 Mt in 2007 and 15 Mt in 2011. Propylene is the second largest raw material [3]. A conventional method for production of olefins is steam cracking. Steam cracking has been the most common method of producing light olefins for 90 years. This method has disadvantages, such as high energy consumption and emissions [1]. Some other methods are catalytic cracking, fluid catalytic cracking (FCC), methanol-to-olefins (MTO) technology, and coal-to-methanol-to-olefin (CTO) [4]. Oxidative dehydrogenation of alkanes includes partial oxidation, oxidative dehydrogenation, and ammoxidation (suggested as an alternative) [5]. Disadvantages of the steam cracking method are low energy efficiency and low selectivity of the desired product. Among the proposed methods, the oxidative dehydrogenation reaction is exothermic, with side products being easily separable. The oxidative dehydrogenation method has not been used in industry [6]. The thermodynamic limitation, the rapid formation of coke, and the high energy consumption are the common problems of conventional processes. Oxidative dehydrogenation of C<sub>2</sub>H<sub>6</sub> with CO<sub>2</sub> as oxidant can be attractive from an industrial and environmental perspective. From an environmental point of view, the use of carbon dioxide as an oxidant reduces the effects of greenhouse gases. The use of a suitable catalyst can overcome the thermodynamic and kinetic barriers of carbon dioxide activation. So far, the appropriate catalysts are H-ZSM-5 supported Cr-catalyst,

Cr/SBA-15, Cr<sub>2</sub>O<sub>3</sub>/ZrO<sub>2</sub>, SiO<sub>2</sub>, Al<sub>2</sub>O<sub>3</sub>, and TiO<sub>2</sub> supported and unsupported Cr catalysts, Ni–Nb–O and Ca doped ThO<sub>2</sub> [7]. HZSM-5 is a microporous, crystalline aluminosilicate zeolite with a regular structure [8]. Zeolites have been used as catalysts in many chemical processes, especially hydrocarbon conversion [9]. Also, properties such as high uniformity, controllable acidic properties, and strong electrostatic field within its cages have attracted much attention [10]. Early theories regarding zeolite showed that the electrostatic field of zeolites leads to their better activity, because catalytic activity increases with the electrostatic field within their cages [11]. By replacing organic cations, which induce electrostatic field gradients within the cages, the activity could be developed [12].

To obtain a high reaction rate, many alternatives have been investigated by researchers, such as plasma technology, applying an external electric field and sono-processing. Applying an external direct current (DC) electric field consumes lower energy compared to plasma [13]. Deren and Mania investigated the role of an external DC electric field in oxidation of carbon monoxide to carbon dioxide on a NiO catalyst and presented a relation between the catalytic performance and electric property of the catalyst surface. Activation energy in the external electric field declined almost about 20 kJ/mole, and energy bands were curved, leading to an increase in the catalytic activity [14]. Andres et al. expressed that the electric field acts as a catalyst in chemical reactions. Ab initio SCF calculations were performed on the fluoride exchange reaction. The results showed that strong electric fields decreased the reaction's activation energy [15]. Sekine et al. studied degradation of ethanol over Pt/CeO<sub>2</sub> catalyst in electric field at 423 K. Thermal analyses indicated that about 90–95% of input power was used in the endothermic reaction [16]. Sekine et al. carried out ethanol steam reformation, dissociation of ethanol, water gas shift, and methane steam reformation in an external DC electric field where the common reaction could barely be activated with conventional methods. In the electric field, feed conversion was drastically increased, and the activation energy was reduced. Feed conversion was drastically enhanced with the DC electric field, and activation energies for these reactions were decreased when utilizing an electric field, and the reaction temperature decreased by about 150 K, as well [17]. Sekine et al. investigated methane steam reforming via metal catalysts supported on CeO<sub>2</sub> and Ce<sub>x</sub>Zr<sub>1-x</sub>O<sub>2</sub> at 423 K. The conversion of CH<sub>4</sub> increased the external electric field, especially for Ce<sub>x</sub>Zr<sub>1-x</sub>O<sub>2</sub> due to the lattice oxygen of Ce<sub>x</sub>Zr<sub>1-x</sub>O<sub>2</sub> [18]. Tanaka et al. studied methane oxidative coupling over SrLa<sub>2</sub>O<sub>3</sub> catalysts at 423 K in the DC external electric field. Electrical conductivity had a key role in the reaction. The highest yield for C<sub>2</sub> (49% selectivity) was achieved with 2.7 W electrical power [19]. Oshima et al. studied the role of input electric current, loading of Pt, and the support properties on the catalytic methane steam reforming in an external electric field at 423 K over CeO<sub>2</sub>, Ce<sub>x</sub>Zr<sub>1-x</sub>O<sub>2</sub> and a mixture of CeO<sub>2</sub> and ZrO<sub>2</sub>, Al<sub>2</sub>O<sub>3</sub> or SiO<sub>2</sub>. The activity increased with input electrical current. Pt/Ce<sub>x</sub>Zr<sub>1-x</sub>O<sub>2</sub> solid had the highest catalytic activity (methane conversion = 40.6% at 535.1 K) [20]. Oshima et al. studied methane oxidative coupling with carbon dioxide in the presence of an electric field through La-ZrO<sub>2</sub>. 5 mol % La-ZrO<sub>2</sub> had the highest catalytic performance, which is attributed to the synergy between La, structure of ZrO<sub>2</sub>, and the external electric field [21]. Oshima et al. studied catalytic reverse water gas shift reaction in the electric field at 423 K. Pt/La-ZrO<sub>2</sub> resulted in the highest yield (40%) [22]. Catalytic water gas shifts for hydrogen production was reported by Sekine et al. at 423–873 K under external electric field over Pt/La-ZrO<sub>2</sub>. Activation energy decreased drastically and the redox mechanism in the lattice oxygen of the surface had a crucial effect in water-gas shift reaction (WGS) reaction in the DC electric field [23]. Methane dry reforming was studied by Yabe et al. over different transition metal-supported ZrO<sub>2</sub> under electric field. 1 wt. % Ni/10 mol % La-ZrO<sub>2</sub> had high activity at 423 K. The electric power consumption was related to the catalytic activity and reaction rate [24]. Yabe et al. investigated methane oxidative coupling by carbon dioxide as oxidant in the electric field at 423 K over different perovskite oxide catalysts. La<sub>0.7</sub>Ca<sub>0.3</sub>AlO<sub>3-δ</sub> had high activity (7.4% C<sub>2</sub> yield at 348 K). The input electrical current was related to the conversion of methane [25]. To determine the mechanism for the steam reforming reaction of CH<sub>4</sub> in the electric field, operando- diffuse reflectance infrared Fourier transform spectroscopy was employed to study CH<sub>4</sub> dissociative adsorption. The results showed that CH<sub>4</sub> was dissociated to

CO, CO<sub>2</sub> when CD<sub>4</sub> and D<sub>2</sub>O were provided instead of CH<sub>4</sub> and H<sub>2</sub>O. The proton collision activated methane at low temperatures in the presence of the DC electric field [26]. Ogo et al. reported methane oxidative coupling and ethane oxidative dehydrogenation using different polyoxometalate-supported CeO<sub>2</sub> at 423 K under external electric field. Tetrabutylammonium salt-supported CeO<sub>2</sub> catalysts had high catalytic activity for these two reactions at 3 mA and 423 K. FTIR and XRD analyses showed that the structure of Tetrabutylammonium salt-supported CeO<sub>2</sub> was transferred to Ce<sub>2</sub>(WO<sub>4</sub>)<sub>3</sub>/CeO<sub>2</sub> after applying an electric field, and it was a proper active site for these two reactions [27]. The oxidative cracking of LPG was investigated in the external DC electric field. CrHZSM-5 had more catalytic activity compared to HZSM-5 and NaZSM-5. According to Faradaic numbers, the reaction progressed electrocatalytically. The best catalytic activity was achieved at 625 °C and 12 mA (olefin yield = 42.58% and LPG conversion = 92.12%) [28].

In this research, a novel catalytic reaction system was investigated for oxidative dehydrogenation of Liquefied Petroleum Gas (LPG) with CO<sub>2</sub> in a DC external electric field over transition metals supported on HZSM-5. Due to the synergy effect of the electric field and electrostatic field gradient in the support catalyst, there is the possibility to improve the catalytic performance. This study is the first report of ethylene and propylene production with the synergetic effect between transition metals impregnated on HZSM-5 and an external electric field. We studied the role of a DC electric field on the HZSM-5 impregnated with transition metal oxides to obtain high catalytic activity. The beneficial use of an external electric field depends on the electronic properties of the catalyst as a semiconductor. These properties include the electrical conductivity, dielectric constant, Fermi surface and band gap of the catalyst. In an effort to explain the relation between catalytic activity and semiconductor property, the modified HZSM-5 with transition metal oxide was characterized by XRD, FTIR, SEM, NH<sub>3</sub>-TPD, H<sub>2</sub>-TPR, BET, TGA, UV-visible, Fermi measurement, Hall and Impedance measurements.

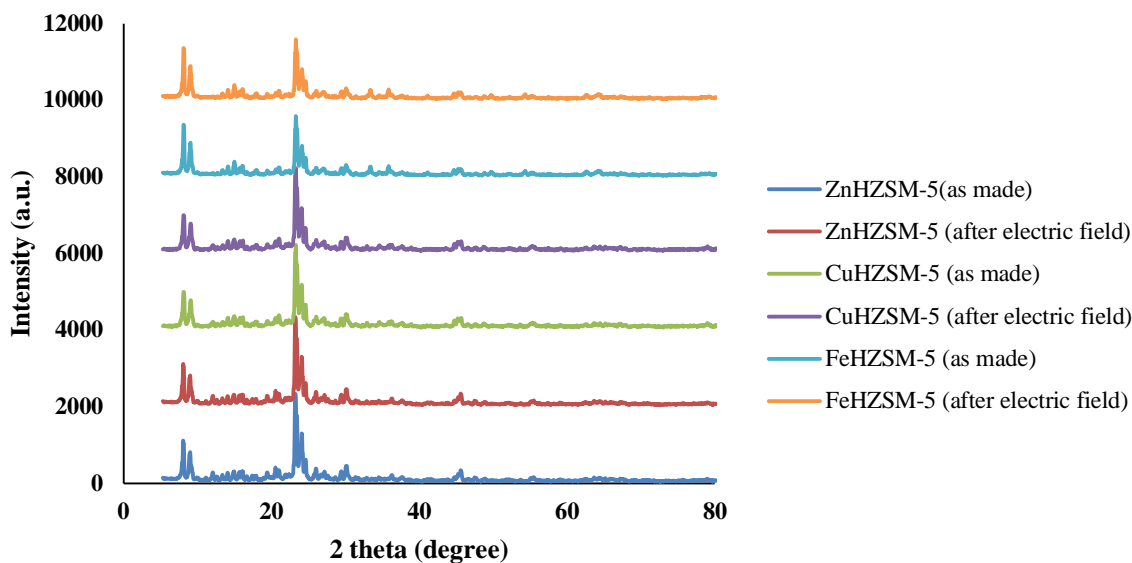
## 2. Results and Discussion

### 2.1. Catalyst Characterization

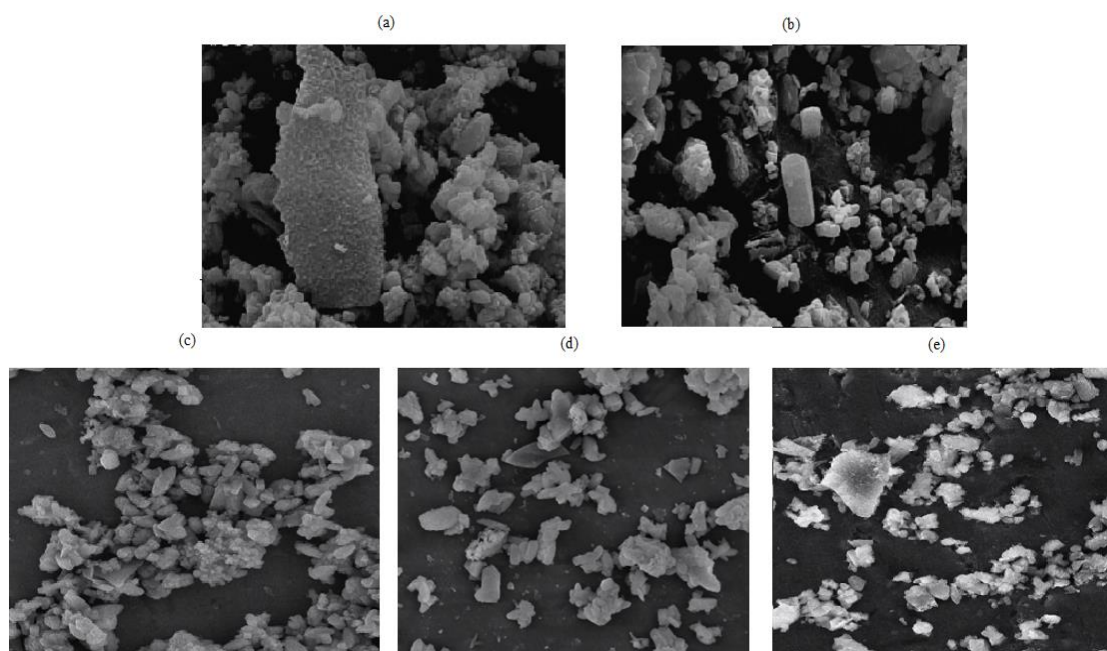
#### 2.1.1. XRD Analysis

Figure 1 shows X-ray diffraction patterns for different catalysts. XRD was analyzed between 5° and 80°. For the impregnated HZSM-5, the XRD patterns were approximately similar to HZSM-5, which shows that the impregnation had no effect on HZSM-5 structure [29]. The structure was intact after treatment, and was Mordenite Framework Inverted (MFI) with characteristic reflections at  $2\theta = 8.0^\circ, 8.9^\circ, 23.1^\circ, 23.4^\circ$  and  $24.0^\circ$ , and no new phase was formed during the treatment. No peak corresponding to the transition metals was observed. The XRD showed that transition metals were well dispersed on HZSM-5. This finding is confirmed by Jiang et al. [30]. Meanwhile, the intensities varied pertaining on the amount of metal. The Cu-impregnated HZSM-5 diffractogram had no relevant peaks at  $36^\circ$  and  $39^\circ$ , corresponding to CuO and Cu<sub>2</sub>O, respectively, which indicated that Cu species were not detected by XRD [31]. The Zn/HZSM-5 catalyst did not show any peaks at  $31.6^\circ, 34.5^\circ, 36.2^\circ$  or  $47.5^\circ$  related to ZnO. Thus, zinc as Zn<sup>2+</sup> is well dispersed in the zeolite framework [32]. Diffraction of the Fe<sub>2</sub>O<sub>3</sub> crystalline structure is  $2\theta = 33.15^\circ, 35.65^\circ, 40.64^\circ, 49.04^\circ$  and  $53.60^\circ$ , which were not detected in the XRD pattern of FeHZSM-5. Therefore, Fe<sub>2</sub>O<sub>3</sub> was well dispersed on the zeolite framework [33]. XRD patterns after reaction are shown in Figure 1. The structures of all catalysts before and after reaction were MFI.

SEM images for zeolites are shown in Figure 2. The zeolites have a hexagonal morphology. Similar results have been observed by other researchers for the synthesized HZSM-5 [34]. In addition to hexagonal crystals, irregular crystals are also observed, which may be due to secondary nucleation reactions. These smaller crystals are adjacent to larger crystals [35]. By comparing Figure 2, it is observed that the particles and structure of zeolite after impregnation with transition metal oxide have not changed, which is also consistent with the XRD results.



**Figure 1.** XRD patterns for NaZSM-5, HZSM-5, 4 wt. %. FeHZSM-5, 4 wt. %. CuHZSM-5 and 4 wt. %. ZnHZSM-5 catalysts in conventional reaction and reaction in the electric field.



**Figure 2.** SEM images for (a) NaZSM-5; (b) HZSM-5; (c) 4 wt. % FeHZSM-5; (d) 4 wt. % CuHZSM-5; and (e) 4 wt. % ZnHZSM-5 catalysts.

### 2.1.2. FTIR Analysis

In Figure 3, the FTIR showed similar spectra for all the catalysts. As can be seen, there was no significant band shift in the spectra for different impregnations. According to the XRD analysis, the zeolite framework remained intact. The FTIR spectral region of ZSM-5 catalysts includes bands at 1225, 1093, 970, 550 and 450  $\text{cm}^{-1}$ , which correspond to external asymmetrical stretching, internal asymmetrical stretching, external symmetrical stretching, double five-membered ring vibration, and T-O bending modes, respectively. Absorption bands of the three catalysts showed the same trend. There was no band around 1398  $\text{cm}^{-1}$ , so all of the chemisorbed ammonium ions during ion exchange treatment were converted to protons after calcination.

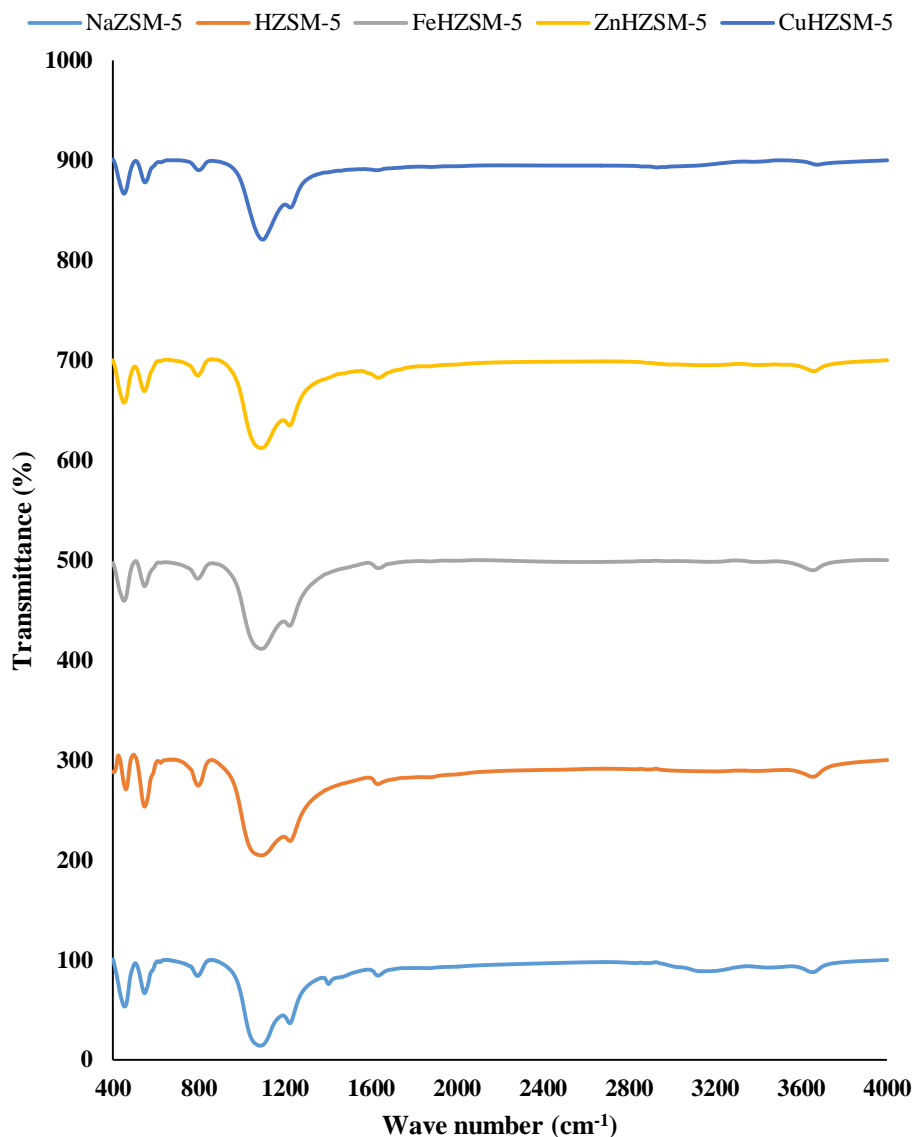


**Figure 3.** Infrared spectra for NaZSM-5, HZSM-5, 4 wt. % FeHZSM-5, 4 wt. % CuHZSM-5 and 4 wt. % ZnHZSM-5 catalysts.

### 2.1.3. BET Analysis

BET results for different catalysts are shown in Table 1. As can be seen, zeolites have a high BET surface area and suitable pore volume. In addition, properties of the prepared samples were close to each other, which suggested that, after impregnation of zeolite with transition metal oxide, the pores and especially the accessible catalyst surface were preserved. To prove this, the nitrogen absorption isotherm is shown for each of the catalysts in Figure 4a, and the isotherms were of type IV. Metal impregnation increased diameter of pores, due to blocking the micropores. Generally, transition metal loading enhances the BET surface area of the HZSM-5. Figure 4b shows the distribution of pore diameter for different HZSM-5 catalysts.

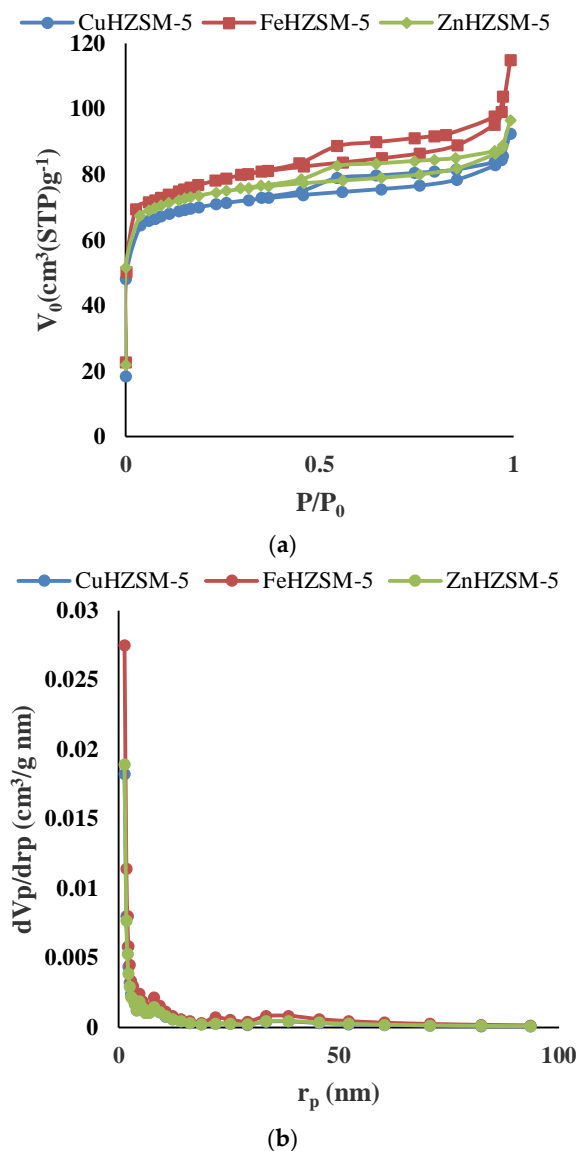


**Figure 4.** (a)  $N_2$  adsorption, desorption for different catalysts 4 wt. % FeHZSM-5, 4 wt. % ZnHZSM-5 and 4 wt. % CuHZSM-5; (b) pore diameter distribution of 4 wt. % FeHZSM-5, 4 wt. % CuHZSM-5 and 4 wt. % ZnHZSM-5 catalysts.

**Table 1.** BET surface area and pore size analysis for all catalyst samples.

Sample	$S_{BET}$ (m <sup>2</sup> /g)	$S_{mic}$ (m <sup>2</sup> /g)	$S_{EXT}$ (m <sup>2</sup> /g)	$V_t$ (cm <sup>3</sup> /g)	$V_{mic}$ (cm <sup>3</sup> /g)	$V_{meso}$ (cm <sup>3</sup> /g)	Average Pore Diameter (Å)
NaZSM-5	206.66	158.60	48.06	0.112	0.088	0.024	21.55
HZSM-5	244.74	163.30	81.44	0.130	0.090	0.040	21.18
4 wt. % CuHZSM-5	274.15	211.17	62.98	0.149	0.103	0.046	21.84
4 wt. % FeHZSM-5	279.27	189.20	90.07	0.175	0.100	0.075	25.53
4 wt. % ZnHZSM-5	274.21	194.83	79.38	0.150	0.103	0.047	21.98

#### 2.1.4. $NH_3$ -TPD Analysis

$NH_3$ -TPD was carried out to study the acid site of different modified HZSM-5 catalysts. Two peaks are present in Figure 5: the low-temperature peak and high-temperature peak are attributed to weak and strong acid sites, respectively [36]. Table 2 presents the acidity amount for different catalysts. The  $NH_3$  desorption peak near 200 °C is ascribed to the weak acid sites of the catalysts [37],

and originated from OH groups on the catalyst surface [38] that were not catalytically important [39]. The second desorption peak was obtained at 350–550 °C, which was surface Brønsted acid [37,40]. 4 wt. % Cu/HZSM-5 had two peaks in the range of 120–280 °C and 300–500 °C. The second site was the main catalytic site for catalytic processes. The NH<sub>3</sub>-TPD for 4 wt. % FeHZSM-5 had two peaks at 100–300 °C and 300–600 °C. The acidity measurement of 4 wt. % Zn/HZSM-5 catalysts showed one peak at 150 to 350 °C and another at 400–550 °C, which were attributed to the low strength of the Lewis and the weak Brønsted acid sites.

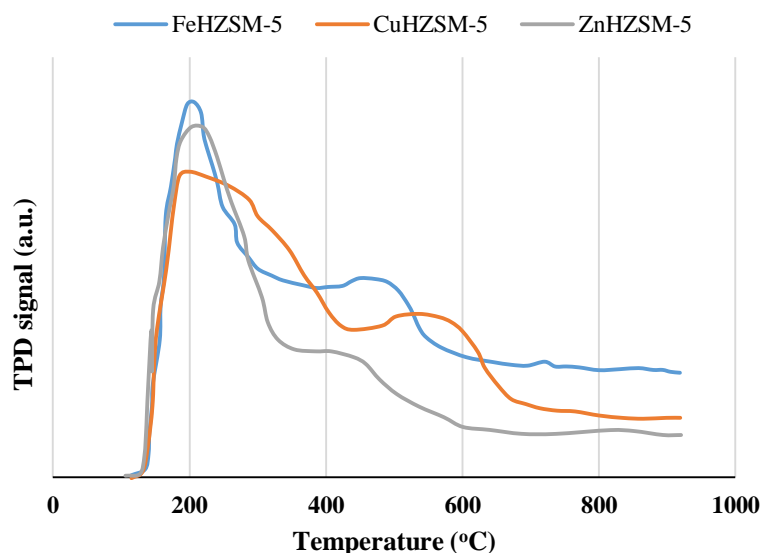


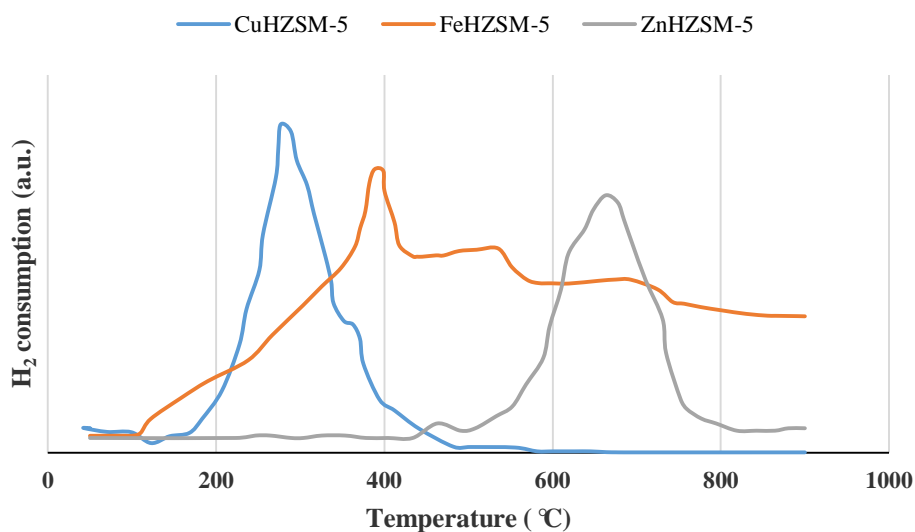
Figure 5. NH<sub>3</sub>-TPD for 4 wt. % FeHZSM-5, 4 wt. % CuHZSM-5 and 4 wt. % ZnHZSM-5 catalysts.

Table 2. NH<sub>3</sub>-TPD results for 4 wt. % FeHZSM-5, 4 wt. % CuHZSM-5 and 4 wt. % ZnHZSM-5 catalysts.

Catalyst	Peak Temperature (°C)		Acidity (mmol NH <sub>3</sub> /g)		Total Acidity (mmol NH <sub>3</sub> /g)
	Weak	Strong	Weak	Strong	
FeHZSM-5	206.947	450.48	0.82	0.70	1.52
CuHZSM-5	200.59	536.94	0.80	0.70	1.50
ZnHZSM-5	202.80	433.25	0.79	0.65	1.44

### 2.1.5. H<sub>2</sub>-TPR Analysis

The H<sub>2</sub>-TPR results are presented in Figure 6. The first reduction peak for CuHZSM-5 was detected at 290 °C (reduction of Cu<sup>2+</sup> to Cu<sup>+</sup>), and it reduced to Cu<sup>0</sup> at 375 °C. The second peak was attributed to the reduction of many particles of copper in the pores. Higher H<sub>2</sub> is needed to reduce the Cu<sup>2+</sup> in the pores [41]. In the impregnation of HZSM-5 with ferrous nitrate, iron was dispersed on HZSM-5 as Fe<sub>2</sub>O<sub>3</sub>. For this catalyst, there were two reduction peaks: the first peak at 300–400 °C was related to the transformation of Fe<sub>2</sub>O<sub>3</sub> to Fe<sub>3</sub>O<sub>4</sub> [42], and the second peak at 400–700 °C was related to reduction of Fe<sub>3</sub>O<sub>4</sub> to Fe<sup>0</sup>. The iron in the lattice was not reducible. The extra crystalline ZnO species reduced at 630 °C [43]. The amount of H<sub>2</sub> consumed was 1.618, 0.902 and 0.759 mmol/g for 4 wt. % FeHZSM-5, 4 wt. % CuHZSM-5 and 4 wt. % ZnHZSM-5, respectively.



**Figure 6.** H<sub>2</sub>-TPR profiles for 4 wt. % FeHZSM-5, 4 wt. % CuHZSM-5 and 4 wt. % ZnHZSM-5 catalysts.

## 2.2. Catalyst Activity

### 2.2.1. Effect of Temperature

The catalytic performance of 4 wt. % CuHZSM-5, 4 wt. % FeHZSM-5 and 4 wt. % ZnHZSM-5 in CO<sub>2</sub> oxidative dehydrogenation of LPG was studied in the DC electric field and conventional reaction. The temperature (T), electric current (I), gap between the two electrodes (GD), metal impregnation (ML), presence of oxidant and contact time (W/F) changed between 575–650 °C, 0–12 mA, 8–14 mm, 2–8 wt. %, CO<sub>2</sub> and 0.64–1.14 g h mol<sup>-1</sup>, respectively.

In the blank case, the external DC electric field had a low catalytic performance, and the maximum LPG conversion and light olefin yield were 11.40% and 3.57%, respectively, at 650 °C. Therefore, the quartz sand had no significant effect on the heterogeneous oxidative dehydrogenation (ODH). Figure 7a,b presents the catalytic activity for different temperatures. As seen from Figure 7a,b, the feed conversion and olefin yield increased drastically with the temperature for all catalysts, since the reaction is endothermic and must provide the activation energy for the feed, resulting in further negative Gibbs free energy at higher temperatures.

In the conventional mode at 650 °C, the maximum LPG conversions for FeHZSM-5, CuHZSM-5 and ZnHZSM-5 were 55.93%, 47.51%, 45.19%, respectively. However, in the presence of the electric field, the maximum conversions for FeHZSM-5, CuHZSM-5 and ZnHZSM-5 were 94.65%, 83.93%, 78.85%, respectively, so the conversion increased by 1.69, 1.76 and 1.74 times when an external electric field was used on the catalyst for FeHZSM-5, CuHZSM-5 and ZnHZSM-5. Light olefin yield over FeHZSM-5 (olefin yield of ca. 48.96%, as well as 64.75% olefin selectivity (Figure S1 in the Supplementary Materials) at 650 °C) is significantly greater than other catalysts, which indicates that the sufficient performance of the FeHZSM-5 can be ascribed to better morphology. The results show that the electric field can increase the catalytic activity of FeHZSM-5 by increasing the adsorption capacity of reactant and surface reaction of these molecules on the catalyst. In all catalysts, only FeHZSM-5 was active, proposing a proper interaction of Fe<sub>2</sub>O<sub>3</sub> and HZSM-5. This may be attributable to the more acidic sites in the Fe metal oxide. The acidic sites activate C-H bonds. The synergy between the high BET surface area and the acidic properties of Fe<sub>2</sub>O<sub>3</sub> enhanced the Fe dispersion and increased the olefin yield. These results are in agreement with an increase in the BET surface area of catalysts loaded with transition metals.

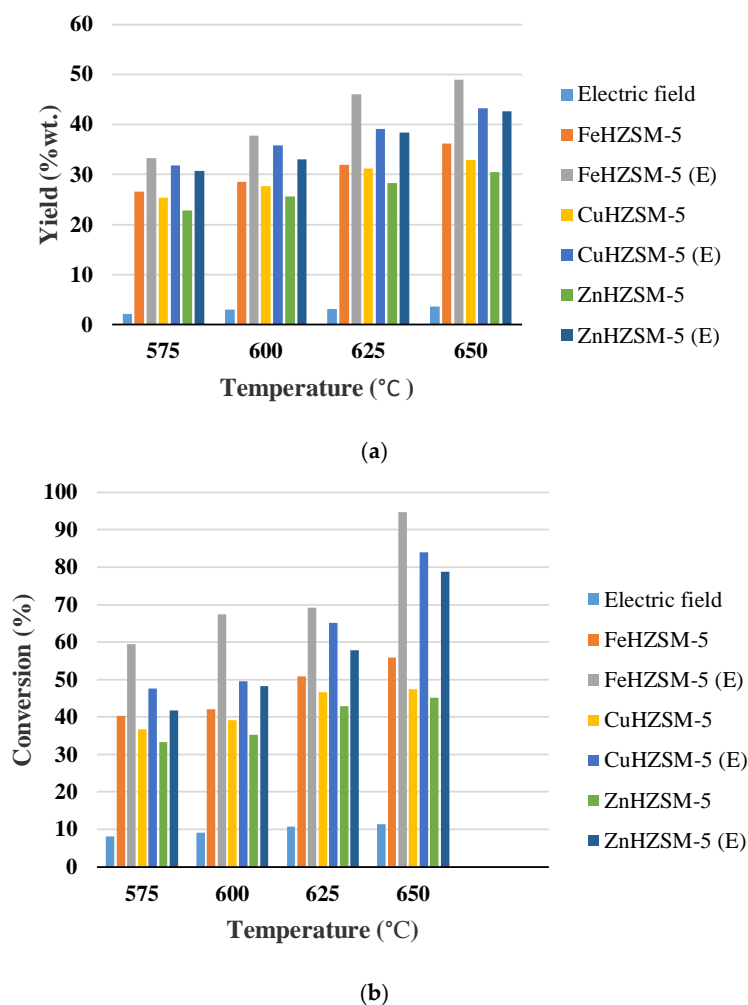


**Figure 7.** Effect of temperature in oxidative dehydrogenation of LPG for 4 wt. % FeHZSM-5, 4 wt. % CuHZSM-5 and 4 wt. % ZnHZSM-5 catalysts on (a) olefin yield; (b) LPG conversion: 100 mg catalyst, 6 mA, 10 mm gap distance and 4 wt. % metal loading.

The TOF (turn over frequency) and productivity are shown in Table 3 and decrease in the following order: FeHZSM-5(E) > CuHZSM-5(E) > ZnHZSM-5(E) > FeHZSM-5 > CuHZSM-5 > ZnHZSM-5. This trend is in accordance with the activation energy calculated by the Arrhenius equation. The various TOFs are attributed to the external electric field and transition metal species. The TOF for FeHZSM-5 with the external DC electric field was greater than the other catalysts, indicating that the active transition metal species in FeHZSM-5 in the electric field is more important to the ODH reaction and olefin formation. The varying activation energy in the conventional reaction and the reaction assisted by the electric field shows that the amount and property of the active sites were altered on the different catalysts. With regard to thermogravimetric analysis (TGA), in the catalytic reaction assisted by external DC electric field, the produced coke declined. The TGA results are shown in Figure 8.

**Table 3.** The TOF (turn over frequency) and productivity for different catalyst in conventional reaction and reaction assisted by electric power: 100 mg catalyst, 6 mA, 10 mm gap distance and 4 wt. % metal loading.

Catalyst	Rate of LPG Conversion (mol LPG g <sup>-1</sup> s <sup>-1</sup> )	TOF (h <sup>-1</sup> )	Apparent Activation Energy E <sub>a</sub> (kJ mol <sup>-1</sup> )	Productivity (g <sub>product</sub> /g <sub>cath</sub> )
ZnHZSM-5	2.16 × 10 <sup>-6</sup>	18.36	177.14	0.21
CuHZSM-5	2.37 × 10 <sup>-6</sup>	20.15	137.83	0.23

Table 3. Cont.

Catalyst	Rate of LPG Conversion (mol LPG g <sup>-1</sup> s <sup>-1</sup> )	TOF (h <sup>-1</sup> )	Apparent Activation Energy E <sub>a</sub> (kJ mol <sup>-1</sup> )	Productivity (g <sub>product</sub> /g <sub>cath</sub> )
FeHZSM-5	2.84 × 10 <sup>-6</sup>	24.15	116.72	0.28
ZnHZSM-5 (E)	3.54 × 10 <sup>-6</sup>	30.10	109.18	0.34
CuHZSM-5 (E)	3.82 × 10 <sup>-6</sup>	32.48	106.15	0.37
FeHZSM-5 (E)	4.05 × 10 <sup>-6</sup>	34.44	87.91	0.40

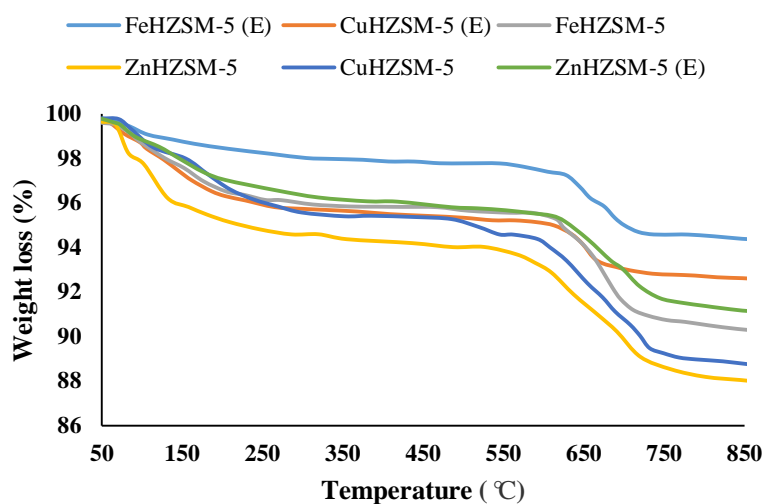


**Figure 8.** TGA analysis of spent 4 wt. % FeHZSM-5, 4 wt. % CuHZSM-5 and 4 wt. % ZnHZSM-5 catalysts in presence and absence of electric field.

To study the catalytic activity of different HZSM-5 catalysts in a DC electric field, the physical-chemical characteristics of the catalysts and the motion of the extra framework of cations are necessary. The motion of these ions results from determining the electrical properties, including electrical conductivity and dielectric constant [44]. The electrical characteristics of various H-ZSM-5 catalysts were investigated at 100 Hz frequency by Impedance Analyzer. HZSM-5 is a dielectric material. In the DC electric field, HZSM-5 saves electrical energy. The DC electric field transmits electrons to the zeolite to achieve the equilibrium state. Relative permittivity ( $\epsilon_r$ ), as a complex number, has both actual and virtual aspects ( $\epsilon_r = \epsilon' - j\epsilon''$ ). The actual ( $\epsilon' =$  permittivity) and virtual ( $\epsilon'' =$  dielectric loss) aspects are stored energy and friction in HZSM-5, respectively. In order to measure these electrical parameters by impedance analysis, a sample pellet is provided with 6.5 mm diameter and 1.2 mm thickness. Then, the catalyst is placed on a ceramic plate and heated at various temperatures for 1 h. After that, the samples are cooled down to 25 °C. The role of temperature on the dielectric constant and dielectric loss are shown in Figure 9a,b.  $\epsilon'$  is enhanced with increasing temperature (Figure 9a). At 650 °C, permittivity had the highest value. Higher temperature increased the motion of the carrier charge [45]. This increase is caused by electrical conduction resulting from the motion of ions in the HZSM-5 cavities, where higher temperatures increase the energy of dipoles [46]. The dielectric loss versus temperature is shown in Figure 9b. Dielectric loss indicates the extraction of power from the DC electric field, which increases with temperature [47]. In general, increases in dielectric constant and dielectric loss increase the carrier charge mobility. Therefore, at 650 °C, in the presence of an external DC electric field, the olefin yield and LPG conversion were enhanced. Electrical conductivity of zeolite is changed by adsorbed species [48]. Electrical conductivity is related to the current carriers [49]. The electrical conductivity mechanism is important in processes in the presence of an electric field [50]. The electric field electrically charges the catalyst surface and leads to the transfer of electrons from the catalyst surface to the reagent, and the charging increases with temperature and dielectric properties [51].

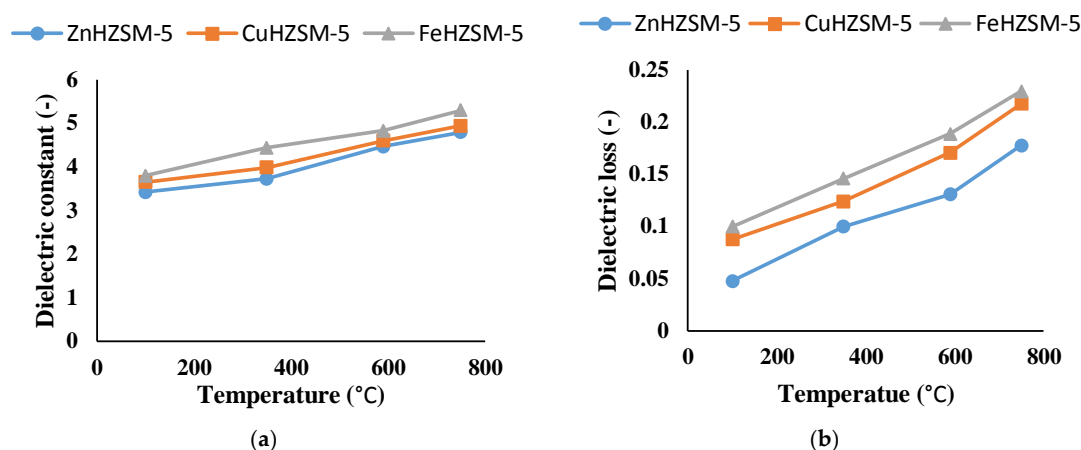


**Figure 9.** The impedance analysis results: (a) Dielectric constant; (b) Dielectric loss versus temperature for different catalysts.

### 2.2.2. Effect of Input Electrical Current

To obtain electrical factors such as input electric current on oxidative dehydrogenation of liquefied petroleum gas with CO<sub>2</sub> in an external electric field, we carried out the activity experiments by changing the input electric currents and measured voltage, and then we calculated the applied electric power. As shown in Table 4, LPG conversion, light olefin yield and selectivity with respect to conversion varied depending on the input current and consumed electric power. These electrical properties change the oxidative dehydrogenation in the external electric field. The input electric current and power are the key electric factors for novel catalytic reaction. When the electric current was changed from 0 mA to 12 mA, the relation between current and voltage was not Ohmic. With an increase in input electrical current, the imposed voltage decreased; however, the electrical power, which is defined as the multiplication of the electric current and the applied voltage, is decreasing. In the conventional reaction, the FeHZSM-5 catalyst has the lowest activity (LPG conv., 50.83%; olefin yield, 31.95%), but in the reaction assisted by the electric field at 12 mA, it had the highest activity (LPG conv., 92.81%; olefin yield, 50.54%). The electric current and electric power affected different adsorbed species and carriers on the catalyst surface. Input electrical current affected the catalytic activity of different transition metals impregnated on HZSM-5 catalysts. Table 4 shows LPG conversion versus input electrical current for different transition metals impregnated on HZSM-5 catalysts. The input electric current increases LPG conversion. As it can be seen in Table 4, by increasing the input electrical current, the olefin production and liquefied petroleum gas conversion increased, and the increase in FeHZSM-5 was greater than ZnHZSM-5 and CuHZSM-5. With an increase in the electric current, the electrons on the catalyst bed were enhanced, enhancing the catalytic activity. The highest olefin yield and LPG conversion were 50.54% and 92.81%, respectively, for 4 wt. % FeHZSM-5 at a temperature of 625 °C and input electrical current of 12 mA. According to Table 4, ZnHZSM-5 had the highest selectivity among all catalysts (73.27%). Table 4 shows light olefin selectivity with different input electric currents. At first, the olefin selectivity increased with the input electric current, and then it decreased with high input electric current. The temperature of the catalyst bed was measured by a thermocouple, which was attached to the lower edge of the catalyst bed in the reactor tube. The furnace reaction temperature was 625 °C, and the reaction temperature measured by the thermocouple on the catalyst bed was 626–631 °C, because of Joule heating by applying the external DC electric field. The temperature of the catalytic bed was slightly increased by the discarded joule heat. Although the furnace temperature was regulated at 625 °C for all input electric current, electrical conductivity increased the temperature in the catalyst bed due to Joule heating. Joule heat changes with the electric power, and the electric power changes with conductivity. Therefore, setting the temperature of the catalyst bed at 625 °C is difficult. The temperature of the catalyst bed is shown in Table 4 with different electric currents.

However, the slight difference in the temperature was negligible. The consumed electric power can increase the catalytic performance, and some of it is converted to Joule heat to enhance the temperature of the catalyst. The Joule heating is not important, as can be seen from empirical data [20].

**Table 4.** Effect of the input electrical current on yield, conversion and selectivity of oxidative dehydrogenation with an external electric field for FeHZSM-5, CuHZSM-5 and ZnHZSM-5 catalysts: 100 mg catalyst sample, 625 °C furnace temperature, 10 mm gap distance and 4 wt. % metal loading.

Catalyst	Input Electrical Current (mA)	Voltage (V)	Temperature (°C)	LPG Conversion (%)	Olefin Selectivity (%)	Olefin Yield (wt. %)
FeHZSM-5	0	0	625	50.83	62.85	31.95
	3	118	626	60.70	63.04	38.27
	6	56	628	69.15	66.63	46.08
	9	37	630	72.07	67.32	48.52
	12	19	631	92.81	54.45	50.54
CuHZSM-5	0	0	625	46.60	66.99	31.22
	3	120	627	56.18	63.74	35.81
	6	59	628	65.16	67.02	39.11
	9	39	629	66.39	66.09	43.88
	12	21	631	74.45	62.88	46.82
ZnHZSM-5	0	0	625	42.88	66.02	28.31
	3	124	626	47.97	73.27	35.15
	6	62	627	57.81	66.35	38.36
	9	41	628	61.24	62.34	38.18
	12	23	629	63.20	60.56	38.28

### 2.2.3. Effect of Gap Distance

The distance between the two electrodes was changed. Figure 10a,b and Figure S2 in the Supplementary Materials illustrate the olefin (ethylene and propylene) yield, feed conversion, and olefin selectivity for various gap distances, respectively. It can be seen in Figure 10, with a decrease in gap distance, that catalytic activity is enhanced. At a temperature of 625 °C, an input electrical current of 6 mA and a metal loading of 4 wt. %, the best olefin yields were achieved with a 8 mm distance between the two electrodes for all catalysts in the catalytic reaction assisted by external electric field; 49.18%, 41.71% and 39.14% for FeHZSM-5, CuHSM-5 and ZnHZSM-5, respectively. According to Figure 10a,b and Figure S2 in the Supplementary Materials, with decreasing gap distance, olefin yield and LPG conversion increased but selectivity decreased.

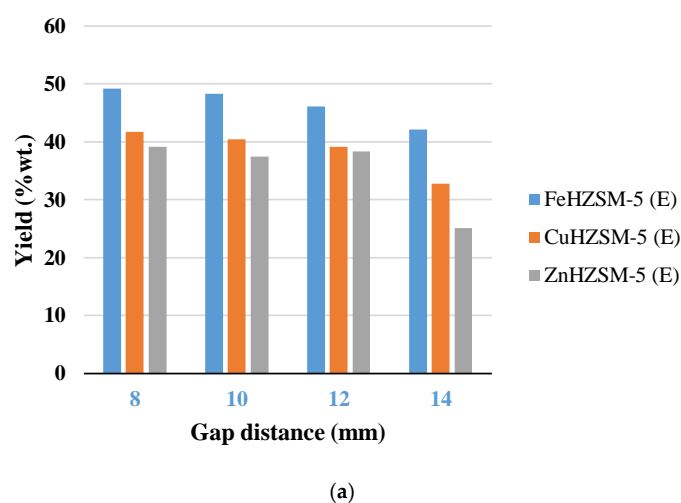


**Figure 10.** Cont.

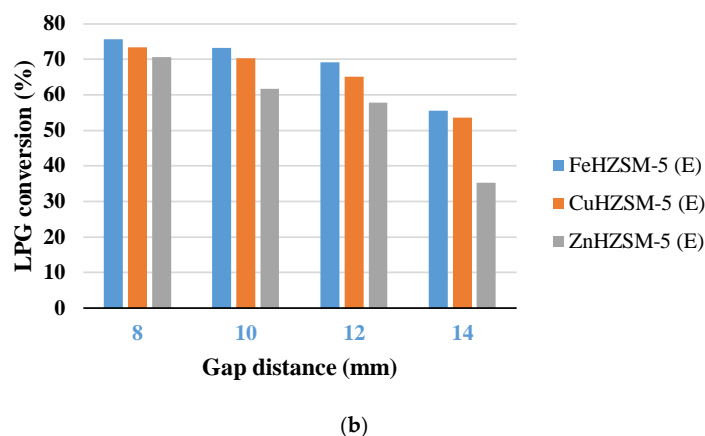


**Figure 10.** Effect of gap distance in oxidative dehydrogenation for FeHZSM-5, CuHZSM-5 and ZnHZSM-5 catalysts on (a) Olefin yield; (b) LPG conversion: 100 mg catalyst, 625 °C, 6 mA, and 4 wt. % metal loading.

#### 2.2.4. The Effect of Metal Loading Amount

According to Figure 11, the electrical conductivity was enhanced significantly with transition metal impregnated on zeolite. Therefore, this property has a key effect on the production of light olefin. Yabe et al. have reported that an electric field can be applied through the catalyst [24]. The substitution of HZSM-5 for divalent transition metal cations ( $\text{Fe}^{3+}$ ,  $\text{Zn}^{2+}$  and  $\text{Cu}^{2+}$ ) increased the carrier mobility, such as holes and oxygen ions. The electrical conductivity of a catalyst is crucial for regulating the conventional reaction in the DC electric field. Borchert and Baern 1997 suggested that doping of strontium in  $\text{La}_2\text{O}_3$  led to an increase in the electrical conductivity of the catalyst [52]. In this research, the impregnation of Cu, Fe, and Zn into HZSM-5 changed the electrical conductivity. Transition metal loading up to 8 wt. % increased the electrical conductivity. Thus, this property had a significant role in the strength of DC field in the formation of ethylene and propylene. Figure 11 presents the electrical conductivity for HZSM-5, 4 wt. % FeHZSM-5, 4 wt. % CuHZSM-5 and 4 wt. % ZnHZSM-5.

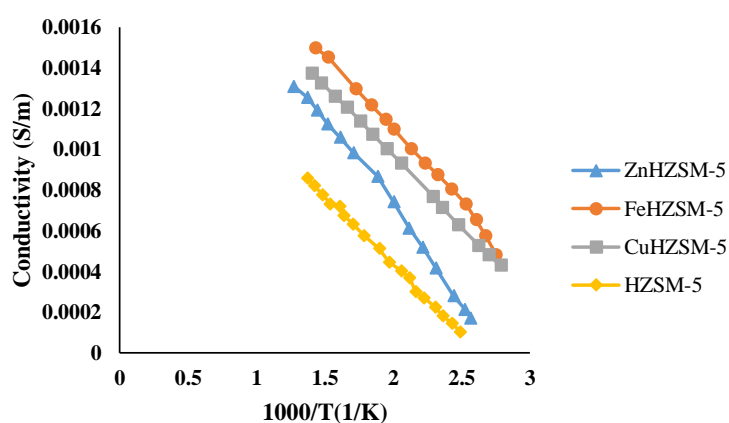


**Figure 11.** Electrical conductivity for HZSM-5, 4 wt. % FeHZSM-5, 4 wt. % CuHZSM-5 and 4 wt. % ZnHZSM-5 catalysts.

Figure 12a,b shows the light olefin yield (propylene and ethylene) and LPG conversion over different content of Zn, Fe and Cu impregnated on the HZSM-5 catalyst in the conventional reaction and reaction in the electric field. The presence of transition metal oxide significantly increased the catalytic performance. The results show that applying an external electric field on the HZSM-5 achieves a proper catalytic activity. This improvement can be attributed to the synergistic effect

between the external electric field and the impregnating metal, the tiny particle, the higher content of the OH groups and the enhancement in the reduction. Also, the transition metal oxide leads to better stability due to supply oxygen species in ODH. The LPG conversion increased with metal loading and the maximum conversion was achieved over HZSM-5 including 8 wt. % Zn, Cu and Fe. A further increase in the metal loading led to an increase in the conversion of LPG. In the DC electric field, the catalyst containing 8 wt. % transition metal oxide had 79.23%, 73.26% and 67.19% LPG conversion for FeHZSM-5, CuHZSM-5 and ZnHZSM-5, respectively, at 625 °C. Small particles, uniform morphology and further active  $M^{n+}$  species lead to better efficiency of the HZSM-5 and enhanced catalytic performance. Impregnation of 8 wt. %  $Fe_2O_3$  as an active site on the HZSM-5 led to a drastic increase in LPG conversion from 54.83% to 79.23% at 625 °C, which can be attributed to the redox property of  $Fe_2O_3$  as shown in the  $H_2$ -TPR analysis. The olefin yield trend was similar to LPG conversion, and FeHZSM-5 catalyst with 8 wt. % metal impregnation had the maximum olefin yield at 650 °C. This catalyst had 49.13% yield at 625 °C, which is an acceptable activity in the ODH. The olefin selectivity (Figure S3 in the Supplementary Materials) was gradually decreased when varying the amount of transition metal.

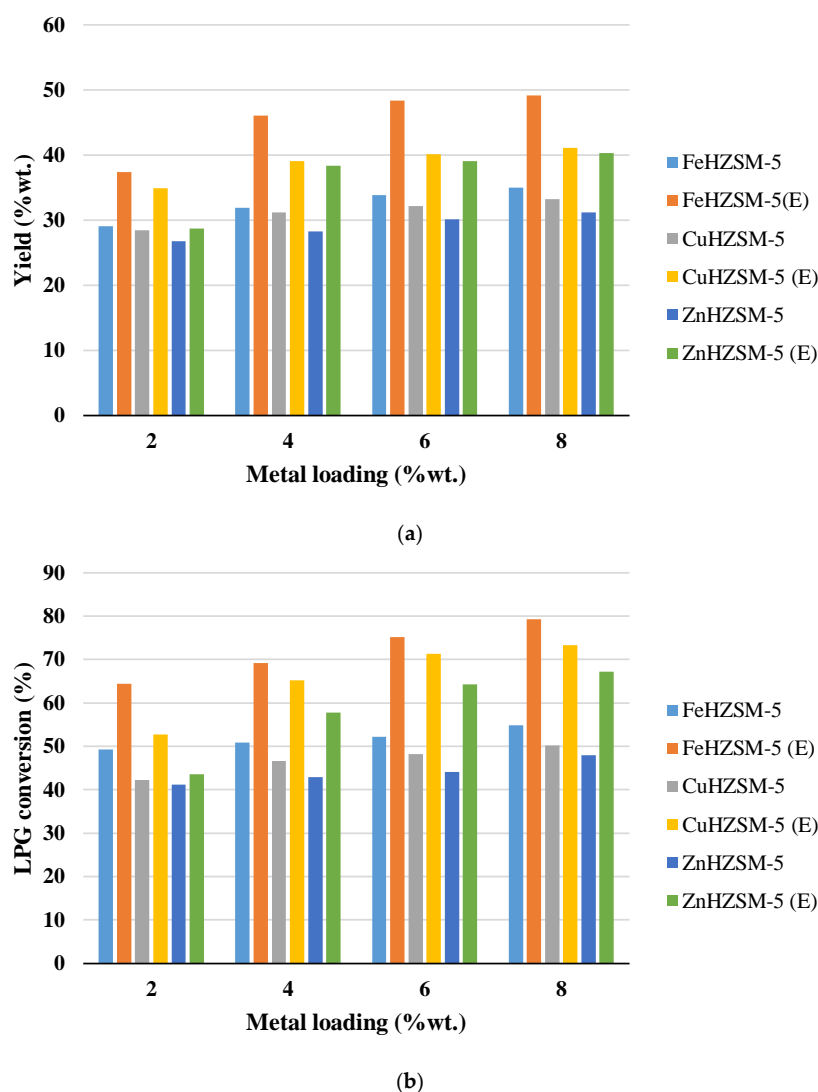


**Figure 12.** Effect of metal loading in oxidative dehydrogenation for FeHZSM-5, CuHZSM-5 and ZnHZSM-5 catalysts in presence and absence of electric field (a) Olefin yield; (b) LPG conversion: 100 mg catalyst, 625 °C, 6 mA, 10 mm gap distance.

When the catalyst surface is in contact with an external electric field with a certain intensity and the electric energy is equal to or more than the band gap, electrons can be transferred from the valence band to the conduction band. Figure 13a shows the UV-visible spectra for various HZSM-5 catalysts ranging between 200 and 1100 nm. Absorption sharply increased at about 200 nm, and after that, it increased gradually. Figure 13b shows  $[F(R_{\infty})h\nu]^{0.5}$  versus photon energy. Extrapolation of these curves determined the optical band gap of the different catalysts. Table 5 shows the electrical properties of the catalyst surfaces. The optical band gap is different for each of the various catalysts. The optical band gap is a criterion for the motion of ions in lattices in the catalyst, which is related to the olefin yield. The band gap affects the activation of lattice oxygen [53]. The band gap decreased with transition metal impregnation and moved toward a lower energy band. The band gap was in the range of 2.35 to 2.95 eV. FeHZSM-5 had the minimum band gap (2.35 eV). The olefin selectivity changed by the mobility of oxygen species of lattice and activation of lattice oxygen in oxidative dehydrogenation of alkanes [54]. According to Table 5, ethylene and propylene yield increases with a decrease in the band gap, due to an increase in mobility of lattice oxygen with band gap. This leads to hydrogen abstraction from alkyl species and ethylene and propylene produced [55]. ZnHZSM-5 had the maximum band gap, so the rate of diffusion for surface oxygen species into lattice of zeolite decreased and the surface adsorbed electrophilic oxygen species increased [56].  $R_H$  (Hall coefficients), for different catalysts that were of the p-type semiconductor, had positive values. By loading with a transition metal, carrier concentration increased. Figure 11 presents the dependency of electrical conductivity on temperature. At 625 °C, electrical conductivity enhanced by metal loading up to 8 wt. % An increase in conductivity with metal impregnation is due to increase in hole concentration.

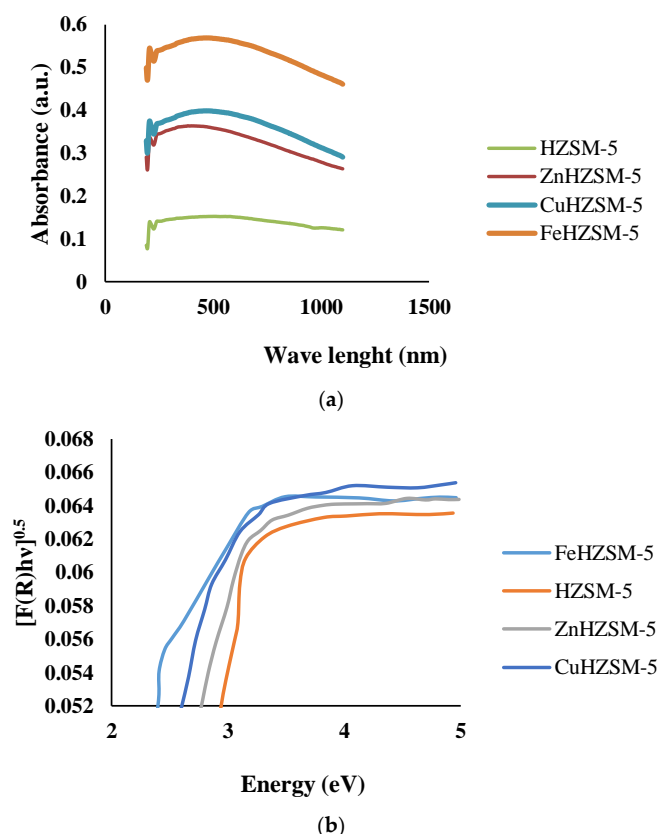


**Figure 13.** (a) Diffuse reflectance UV–visible absorption spectra for HZSM-5, 4 wt. % FeHZSM-5, 4 wt. % CuHZSM-5 and 4 wt. % ZnHZSM-5 catalysts; (b) Graphical of  $[F(R_{\infty})h\nu]^{0.5}$  versus E for 4 wt. % FeHZSM-5, 4 wt. % CuHZSM-5 and 4 wt. % ZnHZSM-5 catalysts to determine the band gap.

**Table 5.** The relation between electrical property and catalytic activity for HZSM-5, 4 wt. % FeHZSM-5, 4 wt. % CuHZSM-5 and 4 wt. % ZnHZSM-5 catalysts.

Catalyst	Band Gap (eV)	F (eV)	$\epsilon(-)$	$P \times 10^{20} (\text{cm}^{-3})$	$F_E$ (eV)	Yield (%)
HZSM-5	2.95	0.64	1.70	3.31	0.68	23.68
4 wt. % FeHZSM-5	2.35	1.14	3.27	4.32	1.47	46.08
4 wt. % CuHZSM-5	2.4	0.94	3.34	3.94	1.15	39.11
4 wt. % ZnHZSM-5	2.8	0.83	3.12	3.33	1.08	38.36

Catalytic performance can be related to Fermi surface. Table 5 shows the Fermi level and electrical properties for alkali and alkaline earth metals impregnated on HZSM-5 catalysts. In the DC electric field, energy bands are curved and the Fermi surface is altered.

$$F_S(E) = F_S + V_S(E) \quad (1)$$

where,  $F_S(E)$  is the Fermi surface in the DC external electric field,  $E$  is the intensity of electric field,  $F_S$  is Fermi surface in the conventional reaction, and  $V_S(E)$  is energy band bending. By inserting the catalyst sample in the DC electric field, reaction was enhanced [14]. Bending energy bands is a function of the intensity of the external DC electric field and an electronic property which is determined as follow:

$$V_S(E) = ELq \quad (2)$$

where,  $q$  and  $L$  are elementary charge and Debye screening length, respectively. Debye screening length is calculated as follows:

$$L = \left( \frac{\epsilon \epsilon_0 kT}{q^2 p} \right) \quad (3)$$

where,  $T$ ,  $k$ ,  $\epsilon$  and  $\epsilon_0$  are the temperature, Stefan Boltzmann constant, dielectric constant of the sample and dielectric constant of vacuum, respectively. Table 5 shows the Fermi level and electronic characteristics in the conventional mode and the reaction in the electric field. As indicated in the electric field, the Fermi level increases and leads to an increase in olefin yield.

### 2.2.5. The Effect of Oxidant

To investigate the role of oxygen species on the catalyst surface in the external DC electric field, reactions were carried out with LPG +  $N_2$  at 625 °C. Figure 14 indicates that  $C_2H_4$  and  $C_3H_8$  were produced over HZSM-5 in the DC electric field without  $CO_2$  oxidant. Therefore, in the DC external electric field, oxygen species were created from metal oxide that was activated with the DC electric field. The interaction between metal oxide and DC electric field forms reactive oxygen species for the dissociation of C–H bond and LPG activation. The oxidative dehydrogenation of LPG in the presence of  $CO_2$  and  $N_2$  is shown in Figure 14, over different catalysts. When  $CO_2$  was employed, the light olefin yield was increased. Generally, the ODH of alkanes over transition metal impregnated on the HZSM-5 progresses the Mars-Van krevelen mechanism; in this mechanism, at first, LPG reduces the surface of the different catalysts by consuming the lattice oxygen, and after that the surface is reoxidized by active oxygen species generated by adsorption of  $CO_2$ .  $H_2$  is released from the surface of the catalyst in the form of  $H_2O$ , so  $CO_2$  enhances the olefin yield. In the presence of  $CO_2$ , the following reactions can occur:



In RWGS (reverse water gas shift reaction), hydrogen consumption increases the LPG conversion. The presence of CO<sub>2</sub> leads to easy elimination of olefins, decrease in coke production. In the presence of inert N<sub>2</sub> only, there are some thermodynamic limitations and no proper olefin yield resulted. In the mode with CO<sub>2</sub>, olefin formed with dehydrogenation and oxidative dehydrogenation. In the oxidative route with CO<sub>2</sub>, the reaction includes reduction of metal species by alkanes and reoxidation of reduced metal by the oxygen species which formed by adsorptive CO<sub>2</sub> dissociation. In this situation, thermodynamic restriction is suppressed. CO<sub>2</sub> in the RWGS reaction eliminates the H<sub>2</sub>. The benefits of CO<sub>2</sub> usage are oxygen species donation and reoxidation of the shortage in lattice oxygen of transition metal and consumption of H<sub>2</sub> in the RWGS reaction.

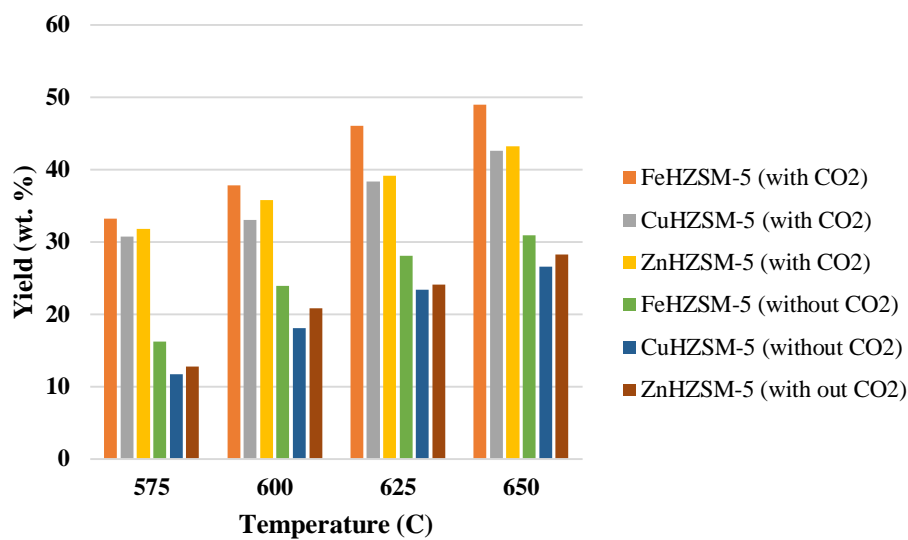


**Figure 14.** Effect of adding carbon dioxide and temperature on Olefin yield for 4 wt. % FeHZSM-5, 4 wt. % CuHZSM-5 and 4 wt. % ZnHZSM-5 catalysts: 100 mg catalyst, 6 mA, 10 mm gap distance and 4 wt. % metal loading.

#### 2.2.6. The Effect of W/F

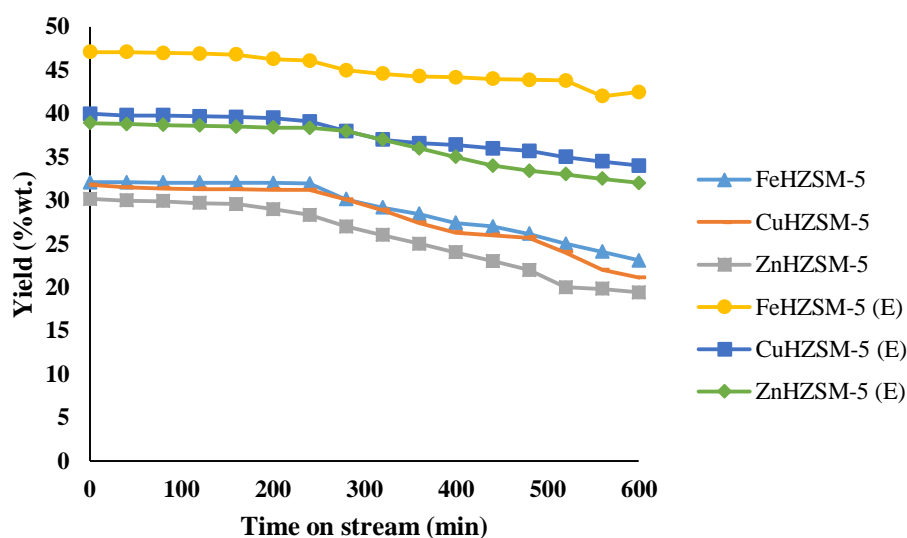
The effect of  $W/F_{LPG}$  on the catalytic activity over different HZSM-5 catalysts at 625 °C in a DC electric field was studied. As shown in Table 6, LPG conversion and light olefin yield increased with contact time. Table 6 indicates LPG conversion and C<sub>2</sub>H<sub>4</sub> and C<sub>3</sub>H<sub>6</sub> selectivity over different HZSM-5 catalysts in a 6 mA DC electric field.

**Table 6.** Effect of  $W/F_{LPG}$  on catalytic activity for FeHZSM-5, CuHZSM-5 and ZnHZSM-5 catalysts: 6 mA electrical current, 10 mm gap distance and 4 wt. % metal loading.

Catalyst	$W/F_{LPG}$ (g h mol <sup>-1</sup> )	Voltage (V)	LPG Conversion (%)	Olefin Selectivity (%)	Olefin Yield (%)
FeHZSM-5	1.14	58	74.37	66.03	49.11
	0.97	56	69.15	66.63	46.08
	0.80	54	66.35	67.70	44.92
	0.64	51	62.18	66.24	41.19
CuHZSM-5	1.14	61	68.15	61.90	42.19
	0.97	59	65.16	60.02	39.11
	0.80	55	63.83	57.85	36.93
	0.64	53	60.74	58.06	35.27
ZnHZSM-5	1.14	63	60.52	68.98	41.75
	0.97	62	57.81	66.35	38.36
	0.80	54	55.42	63.67	35.29
	0.64	54	52.18	62.99	32.87

### 2.2.7. Time on Stream

The stability of the FeHZSM-5, ZnHZSM-5 and CuHZSM-5 containing 4 wt. % metal loading was investigated at 625 °C in the conventional reaction and reaction assisted by external DC electric field. Figure 15 shows the time on stream over 10 h. With an increase in the time on stream, the LPG conversion and light olefin yield decreased gradually, due to coke formation and the reduction in the redox metal species. The decrease in the reaction assisted by the electric field was smaller than observed by TGA analysis. For these catalysts, LPG conversion and light olefin decreased. In the reaction assisted by electric field, LPG conversion and olefin yield declined from 70.36% and 47.10% to 60.5% and 42.5%, respectively, over 4 wt. % FeHZSM-5 after 10 h reaction. In the reaction assisted by an external electric field mode, all catalysts were stable up to 600 min (4.6% decrease in the yield and 9.86% decrease in conversion for 4 wt. % FeHZSM-5), but in the conventional reaction, the stability was lower (8.72% decrease in yield and 18.25% decrease in conversion for 4 wt. % FeHZSM-5). Fe<sub>2</sub>O<sub>3</sub> enhances the thermal stability of the catalyst. The better interaction between active species and the HZSM-5 support assists in avoiding deactivation. The rate of deactivation in the conventional reaction was higher than that in the presence of the external DC electric field. All catalysts had acceptable performance after 600 min of time on stream, probably due to using the external electric field on the catalyst bed, which activates further active sites. These results are related to the better dispersion of ferrous oxide on the surface of the HZSM-5 support. In the impregnation of different transition metals on the HZSM-5, Fe<sub>2</sub>O<sub>3</sub> had higher de-coking and further oxygen mobility and oxygen capacity. The deactivation of the catalyst is attributed to coke formation and the deep reduction of transition metal oxide. The stability is attributed to the properties of the surface catalyst and donor of oxygen in the reaction assisted by the DC electric field. Perhaps, in the external DC electric field, further interaction between the transition metal species and the HZSM-5 support and the ability of the support to donate oxygen species lead to further oxygen mobility, and the reoxidation of reduced metal species suppresses the deactivation of the catalyst. In the FeHZSM-5, the presence of smaller tiny particles and the de-coking property of Fe led to higher stability. The further mesoporous decrease in the resistance to heat and transfer led to better catalytic performance. This proper stability is attributed to the presence of small particles, good BET surface area, and sufficient content of the active M<sup>n+</sup> species and OH groups detected in the FTIR.



(a)

Figure 15. Cont.

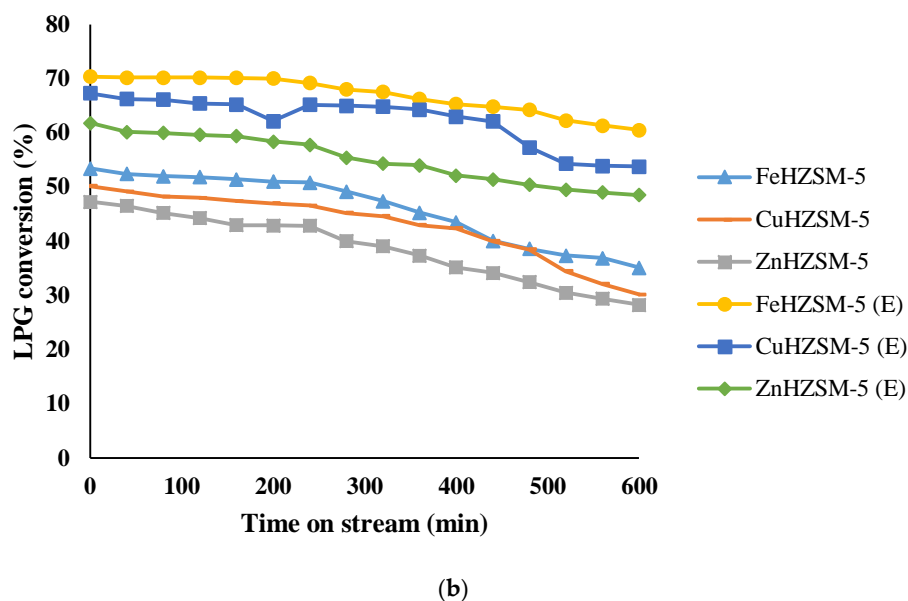


**Figure 15.** Effect of time on stream in oxidative dehydrogenation for 4 wt. % FeHZSM-5, 4 wt. % CuHZSM-5 and 4 wt. % ZnHZSM-5 catalysts in the presence and absence of electric field: (a) Olefin yield; (b) LPG conversion: 100 mg catalyst, 625 °C, 6 mA, 10 mm gap distance and 4 wt. % metal loading.

### 2.2.8. The Mechanism of Oxidative Dehydrogenation of LPG in an Electric Field

The products were  $C_2H_4$ ,  $C_3H_8$ ,  $C_2H_2$ , alkanes, CO, and  $CO_2$ . FeHZSM-5 had a high light olefin yield, which suggested that the C–H bond of  $C_3H_8$  and  $C_4H_{10}$  were further dissociated, rather than C–C bond in the electric field. LPG conversion increased with input electrical current or contact time (W/F), the  $C_2H_2$  selectivity was low in the entire range of LPG conversion. Therefore, the oxidative dehydrogenation of LPG to light olefin was promoted and the dehydrogenation of light olefins to  $C_2H_2$  was an unfavorable side reaction.

At first, alkanes (propane and butane) are adsorbed on the catalyst surface (removal of H atom generates surface alkyl or alkoxide and hydroxyl groups), and then react with lattice oxygen, and transition metals are reduced and react with  $CO_2$ , which is adsorbed and dissociated on the catalyst surface. Light olefin is produced with direct dehydrogenation and oxidative dehydrogenation. The fracture of C–H is the rate determining step. The alkoxide species which are adsorbed are accompanied by  $\alpha$ -hydrogen or  $\beta$ -hydrogen abstraction. These steps lead to olefin and aldehyde. The rupture of the C–C bond in the aldehyde species and C=O bond generation can form alkyl species and surface formyl. Oxidation of formyl species with active oxygen species forms CO,  $CO_2$  and  $H_2O$ .  $\beta$ -hydrogen abstraction proceeds with the Brønsted acid site of HZSM-5. According to the  $NH_3$ -TPD results,  $\beta$ -hydrogen abstraction is dominant. This corresponds to the amount of olefin.  $CO_2$  is decomposed to CO and oxygen species (O). The active oxygen adsorbed by the vacancy of oxygen ( $[O]$ ), in order for the generation of lattice oxygen and the oxidation of the reduced transition metal species to take place, and the cycle finished. The dehydrogenation occurs on the reduced transition metal species. Despite oxidation of some of the reduced transition metal species with oxidant, the association of the reduced species occurs gradually and leads to a decrease in catalytic performance. Alkane cracking is the most probable sidelong reaction.

For semiconductors which are used as a catalyst, the band gap, the conduction band and the valence band have a crucial role in the catalytic conversion. Figure S4 in the Supplementary Materials shows the band gap and potentials of the valence and conduction bands for transition metal oxides as semiconductor based on a potential scale (V) and the normal hydrogen electrode (NHE), as well as the redox potentials of the different species that can be produced in the oxidative dehydrogenation of LPG and  $CO_2$ .

In order to make the process of applying external electric field effective on a catalytic bed, the electro-generated electrons in the conduction band edge must have a more negative potential compared to the redox potential of the CO/CO<sub>2</sub> so that they have enough energy to reduce the absorbed molecules of CO<sub>2</sub> (LPG) to alkanes, alkenes and oxygenates. Also, the potential of the electro-generated holes in the valence band must be more positive compared to the product/alkanes redox potential in order to produce protons, oxygen, alkanes and olefins. Therefore, the band gap of the electro-catalyst should change the redox potential. Semiconductor materials with band gaps in the range of 1.7 to 3.1 eV are suitable catalysts, having enough energy for the excitation of electron-hole pairs. A catalyst with a smaller band gap has better catalytic efficiency due to the minimum wavelength needed to excite the electron-hole pairs.

The proposed mechanism of LPG oxidative dehydrogenation with CO<sub>2</sub> as oxidant is shown in Figure 16. When an external electric field is applied on the catalyst bed, which has an energy greater than the band gap ( $E_g$ ) of the transition metal oxides impregnated on the HZSM-5, the electrons located in the valence energy band are moved to the conduction energy band (CB), so holes are created in the valence band (VB). Electro-generated electron-hole pairs are separated, and move to active sites at the catalyst interface and then react with chemicals (e.g., CO<sub>2</sub> and LPG). Holes in the valence band edge (with high oxidation potential) oxidize alkanes to O<sub>2</sub>, alkanes, alkenes and oxygenates, and electrons in the conduction band edge on the catalyst surface reduce CO<sub>2</sub> to other chemicals, such as CO.

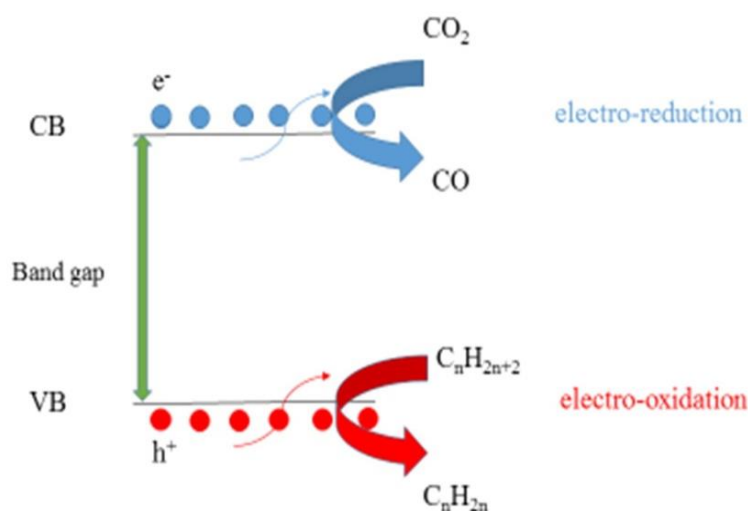


**Figure 16.** Proposed mechanism for oxidative dehydrogenation of LPG under external electric field.

To study the catalyst activity in the DC external electric field, the catalytic performance and stability were investigated with respect to other catalysts in previous research with LPG as feedstock. However, their reaction conditions were different. Table 7 shows the different zeolite catalysts in the ODH of LPG. The yield of light olefins was used to compare this work with previous research. The reaction conditions were different. HZSM-5 in Ref. [57] had the minimum yield for ethylene and propylene production, and based on Table 7, FeHZSM-5 in the presence of DC electric field had the maximum olefin yield; also, the stability of FeHZSM-5 was greater in the DC external electric field. In general, an external electric field can be used on FeHZSM-5 in the oxidative dehydrogenation of LPG.

**Table 7.** Comparison of catalyst activity with previous works.

Catalyst	Temperature (°C)	W <sub>cat</sub> (g)	Feed Composition (cc/min)	Si/Al	TOS (min)	Yield	Reference
P/St/HZSM-5	650	0.2	LPG/N <sub>2</sub> = 25/25	30	240	46.72	[58]
HZSM-5	650	0.2	LPG/N <sub>2</sub> = 25/25	30	120	40.13	[57]
HZSM-5 CNT(30)	650	0.12	LPG/N <sub>2</sub> = 25/25	30	140	46	[34]
(4 wt. %) FeHZSM-5	650	0.1	LPG/CO <sub>2</sub> /N <sub>2</sub> = 10/40/10	14	360	50.54	-

### 3. Materials and Methods

#### 3.1. Catalyst Preparation

The Na-form of ZSM-5 zeolites (Si/Al = 14) was converted into HZSM-5 by three times ion-exchange in 100 mL of NH<sub>4</sub>NO<sub>3</sub> solution (1 M) for 3 h at 80 °C, filtered with Buchner funnel, and washed with distilled water. Then, it was dried at 110 °C in an oven overnight. Consequently, the sample was calcined in a furnace at 823 K for 5 h, under airflow. All transition metal oxides loaded on HZSM-5 were provided by an impregnation wetness procedure with a solution of metal precursor and an oxide support. For impregnation of a transition metal—such as Fe, Cu, and Zn metals—onto the HZSM-5 support, a metal precursor (for Fe, Fe(NO<sub>3</sub>)<sub>3</sub>·9H<sub>2</sub>O, for Cu, Cu(NO<sub>3</sub>)<sub>2</sub>·3H<sub>2</sub>O, for Zn, Zn(NO<sub>3</sub>)<sub>2</sub>·4H<sub>2</sub>O) was used as a solution. The content of transition metal oxides on the HZSM-5 was variable between 2 to 8 wt. %. To the extent necessary, weights of HZSM-5 and Fe(NO<sub>3</sub>)<sub>3</sub>·9H<sub>2</sub>O, Cu(NO<sub>3</sub>)<sub>2</sub>·3H<sub>2</sub>O and Zn(NO<sub>3</sub>)<sub>2</sub>·4H<sub>2</sub>O were introduced to distilled water (100 mL) at 25 °C. After that, the slurry was well stirred for 3 h. Thereafter, the slurry was dried with vacuumed rotary at 110 °C overnight for 12 h; eventually, the catalysts were calcined under air at 650 °C for 6 h.

#### 3.2. Characterization

XRD patterns of the catalyst were obtained by PHILIPSPW1730 (Philips, Eindhoven, Netherlands) using Cu K $\alpha$  radiation in the range of  $2\theta = 5\text{--}80^\circ$ . SEM (Hitachi, Tokyo, Japan) was performed to investigate the morphology of the catalysts by Hitachi S-4160 SE. The surface functional groups were studied with FTIR analysis by Perkin Elmer spectrophotometer version (PerkinElmer, Waltham, MA, USA) (10.03.06) between 400 to 4000 cm<sup>-1</sup>. BET was carried out with Micromeritics (US) apparatus (BEL Corp., Osaka, Japan). The t-plot method determined the micropore volumes and BET surface areas and the pore size of each catalyst was determined by the BJH approach. NH<sub>3</sub>-TPD analysis (BEL, Osaka, Japan) was performed to determine the acidity with a BELCAT apparatus. At first, the sample was degassed at 550 °C for 2 h and then cooled to 100 °C, the injection flow rate of ammonia was 2.5 cm<sup>3</sup>·min<sup>-1</sup> with 10 °C min<sup>-1</sup> temperature ramp. In order to remove the ammonia, the catalyst was flushed in a He stream for 30 min at 100 °C. For H<sub>2</sub>-TPR, at first, a 50 mL/min He stream was passed through the catalyst for 1 h at 200 °C and after that cooled to 25 °C. H<sub>2</sub>-Argon was introduced to the catalyst at 50 mL/min and then the temperature was raised from 25 °C to 650 °C with 20 °C/min. Hydrogen uptake was detected by a TCD (Agilent, Santa Clara, CA, USA). The amount of coke formation on the catalyst after reaction in the conventional method and in the reaction assisted by electric power was analyzed by thermo gravimetric method (TGA). The temperature of the catalyst was raised in the air stream from 25 °C to 1000 °C. Heating rate was 10 °C/min. IM6eX; Zahner-elektrik GmbH & Co. KG impedance analyzer (ZAHNER-Elektrik, Kronach, Germany) determined the electrical conductivity. The impedance analysis was carried out in Ar atmosphere and reaction conditions. The optical band gap was determined with UV-Vis spectrophotometer (Agilent, Santa Clara, CA, USA) (Varian Cary 100). The optical absorption bands were in the range of 200–1100 nm. The bang gap was measured using the Kubelka–Munk (K–M or FI) approach (Equation (9)):

$$F(R_\infty) = \frac{(1 - R_\infty)^2}{2R_\infty} \quad (9)$$

where  $R_\infty$  is the ratio between reflectance of sample and blank. The band gaps for different samples can be calculated by plotting  $[F(R_\infty)h\nu]^{0.5} - h\nu$ . The energy band gap ( $E_g$ ) was obtained by extrapolating slope of the graph [59].

Fermi level was measured with the insertion of two ends of each catalyst, at different temperatures, in a thermally insulated reservoir containing water baths, cold-water baths, or dry ice-alcohol mixtures. The temperature was reported using thermocouples. In addition, the voltage difference between the two ends of the samples was determined by a voltmeter. Fermi level is determined as follows:

$$\text{p-type semiconductor: } TQ_p e = (E_f - E_v) + 2kT \quad (10)$$

$$\text{n-type semiconductor: } -TQ_n e = (E_c - E_v) + 2kT \quad (11)$$

where,  $E_F$ ,  $k$ ,  $E_v$ ,  $E_c$ ,  $e$  and  $Q$  are Fermi level, Boltzmann's constant, energy of valence band, energy of conduction band, electric charge, and thermoelectric power, respectively. Thermoelectric power can be determined as follows [60].

$$Q = -\frac{dV}{dT} = -\frac{\Delta V}{\Delta T} = -\frac{\Delta V}{(T_2 - T_1)} \quad (12)$$

The measurement of the Hall coefficient was used to determine the current carrier concentration at 25 °C with a PPMS system. At 300 K, carrier concentration was determined by  $e$  and  $R_H$  ( $1/eR_H$ ),  $e$  and  $R_H$  are elementary electric charge and hall coefficient, respectively [61]. Impedance measurements were used for dielectric constant measurement. Catalysts with a diameter of 30 mm and thickness of 3 mm were provided. The catalyst was placed between two copper circular disks. The permittivity ( $\epsilon'$ ) and loss factor ( $\epsilon''$ ) of dielectric constant were corresponded to the phase angle ( $\varnothing$ ) and impedance ( $Z$ ) as follow:

$$\epsilon' = \frac{Z_i}{2\pi f C_0 Z^2} \quad (13)$$

$$\epsilon'' = \frac{Z_f}{2\pi f C_0 Z^2} \quad (14)$$

where,  $f$  is frequency,  $C_0$  ( $C_0 = \epsilon_0 A/T$ ) is electrode capacitance,  $T$  is thickness of the disk,  $A$  is surface area of the disk, and  $\epsilon_0$  is free space permittivity.  $Z_i$  and  $Z_r$  are the imaginary and real parts of the complex impedance, respectively [62].

### 3.3. Catalytic Test

Catalytic experiments were performed in a DC external electric field using a quartz reactor (15 mm o.d.) reactor. The schematic plot of the reactor in the electric field is shown in Figure S5 in the Supplementary Materials. Two stainless perforated electrodes were inserted at the top and bottom of the catalysts. In each experiment, the transition metal oxides were loaded on HZSM-5 (100 mg) and diluted with 500 mg silica and were fed to the center of the quartz tube. For oxidative dehydrogenation of liquefied petroleum gas using  $\text{CO}_2$  in an external electric field through transition of metal oxides supported on HZSM-5, feed flow rate was  $\text{LPG}:\text{CO}_2:\text{N}_2 = 10:40:10$  ( $60 \text{ mL min}^{-1}$ ). One thermocouple in the catalyst bed was used to measure temperature. A DC power supplier was used to create an external electric field on the catalyst bed and this electric field with two electrodes was applied to each ends of the catalyst bed. The external electric field was controlled by input electrical current. The voltage pertains to the electronic attributes of the samples and the dielectric characteristic of the feed gas. In the experiments, for comparison between the conventional method and the use of the external electric field, the temperature was changed from 575 to 650 °C. The employed current electric field was in the range of 0–12 mA. After reaction,  $\text{CH}_4$ ,  $\text{CO}$ ,  $\text{CO}_2$ ,  $\text{C}_2\text{H}_4$ ,  $\text{C}_2\text{H}_6$ ,  $\text{C}_3\text{H}_8$ ,  $\text{C}_4\text{H}_{10}$ ,  $\text{C}_2\text{H}_4$ ,  $\text{C}_3\text{H}_6$ ,  $\text{C}_3\text{H}_8$  were detected with a GC-FID (GC-2014; Shimadzu Corp., Kyoto, Japan) as well as

GC-TCD for H<sub>2</sub> analysis. LPG conversion, selectivity of light olefin, and olefin yield were obtained with the following equations:

$$\text{Conversion of LPG} = \frac{\text{weight of LPG reacted}}{\text{weight of LPG initial}} \quad (15)$$

$$\text{Yield of light Olefin} = \text{The total wt. \% of ethylene and propylene} \quad (16)$$

$$\text{Selectivity of light Olefins} = \frac{\text{Yield of light Olefins}}{\text{Conversion of LPG}} \quad (17)$$

#### 4. Conclusions

Oxidative dehydrogenation of liquefied petroleum gas with CO<sub>2</sub> was studied in the conventional reaction and a reaction assisted by an external DC electric field over transition metal impregnated on HZSM-5. Due to the synergy effect of the electric field and the electrostatic field gradient in the support catalyst, there is the possibility to improve catalytic performance. FeHZSM-5 had higher activity than ZnHZSM-5 and CuHZSM-5. All zeolite catalysts were stable after the reaction, in the electric field and BET specific surface area remained unchanged. In the reaction assisted by electric field mode, coke deposition decreased. The conversion increased by 1.69, 1.76 and 1.74 times when an external electric field was used on the catalyst for FeHZSM-5, CuHZSM-5 and ZnHZSM-5. The TOF for FeHZSM-5 in external DC electric field was greater than the other catalysts. The electric field electrically charged the catalyst surface and led to the transfer of electrons from the catalyst surface to the reagent and a charging increase with temperature and dielectric properties. High input electrical current provided more electrons in the reaction and developed the catalytic reaction. The synergistic effect of the catalyst and an external electric field were observed in the minimum gap distance between the two electrodes. The electrical conductivity increased with transition metal loading on the HZSM-5 support. Catalytic performance was greater in the presence of CO<sub>2</sub> instead of N<sub>2</sub> and higher W/F<sub>LPG</sub>. The band gap of each catalyst, as a semiconductor, is a criterion for studying the promotion of the catalytic process. In the reaction assisted by an electric field on the catalyst surface, the surface charge increases, leading to curvature in the energy band. This phenomenon increases the Fermi level. Generally, with higher transition metal loading and higher external electric field, Fermi level increases and catalytic process proceeds. The ethylene and propylene yield increases with the decrease in the band gap due to increases in mobility of lattice oxygen with band gap. This led to hydrogen abstraction from alkyl species and ethylene and propylene being produced. FeHZSM-5 in the presence of the DC electric field had the maximum olefin yield; also, the stability of FeHZSM-5 was greater in the DC external electric field compared to the zeolites studied in previous studies in the absence of electric field. The results indicated an external electric field significantly cracked liquefied petroleum gas to ethylene and propylene at temperature of 650 °C and input electrical current of 12 mA, and it led to 50.54% olefin yield, 92.81% conversion, respectively, over FeHZSM-5.

**Supplementary Materials:** The following are available online at <http://www.mdpi.com/2073-4344/8/7/270/s1>, Figure S1: Effect of temperature on oxidative dehydrogenation of LPG for 4 wt. % FeHZSM-5, 4 wt. % CuHZSM-5 and 4 wt. % ZnHZSM-5 catalysts on selectivity in presence and absence of electric field: on olefin selectivity: 100 mg catalyst, 6 mA, 10 mm gap distance and 4 wt. % metal loading, Figure S2: Effect of gap distance on oxidative dehydrogenation for 4 wt. % FeHZSM-5, 4 wt. % CuHZSM-5 and 4 wt. % ZnHZSM-5 catalysts on olefin selectivity: 100 mg catalyst, 625 °C, 6 mA, and 4 wt. % metal loading, Figure S3: Effect of metal loading on oxidative dehydrogenation for 4 wt. % FeHZSM-5, 4 wt. % CuHZSM-5 and 4 wt. % ZnHZSM-5 catalysts on olefin selectivity: 100 mg catalyst, 625 °C, 6 mA, and 10 mm gap distance, Figure S4: Band gap, potentials of valence and conduction bands of various semiconductor metal oxides, Figure S5: The schematic of fixed bed flow type reactor in the electric field.

**Author Contributions:** In this paper, A.A. designed the experiments; A.A. performed the experiments; A.A. analyzed the data; the manuscript was written by A.A. and edited by R.K.

**Funding:** This research received no external funding.

**Conflicts of Interest:** The authors declare no conflict of interest.

## References

1. Sadrameli, S.M. Thermal/catalytic cracking of liquid hydrocarbons for the production of olefins: A state-of-the-art review II: Catalytic cracking review. *Fuel* **2016**, *173*, 285–297. [[CrossRef](#)]
2. Xiang, Y.; Zhou, J.; Lin, B.; Xue, X.; Tian, X.; Luo, Z. Exergetic evaluation of renewable light olefins production from biomass via synthetic methanol. *Appl. Energy* **2015**, *157*, 499–507. [[CrossRef](#)]
3. Xiang, D.; Gao, L.; Liu, X.; Guo, C.; Yang, S.; Qian, Y. Water consumption analysis of olefins production from alternative resources in China. *J. Clean. Prod.* **2016**, *139*, 146–156. [[CrossRef](#)]
4. Usman, A.; Abdul Bari Siddiqui, M.; Hussain, A.; Aitani, A.; Al-Khattaf, S. Catalytic cracking of crude oil to light olefins and naphtha: Experimental and kinetic modeling. *Chem. Eng. Res. Des.* **2017**, *120*, 121–137. [[CrossRef](#)]
5. Ishchenko, E.V.; Gulyaev, R.V.; Kardash, T.Y.; Ishchenko, A.V.; Gerasimov, E.Y.; Sobolev, V.I.; Bondareva, V.M. Effect of Bi on catalytic performance and stability of MoVTeNbO catalysts in oxidative dehydrogenation of ethane. *Appl. Catal. A Gen.* **2017**, *534*, 58–69. [[CrossRef](#)]
6. Bortolozzi, J.P.; Portela, R.; Ávila, P.; Milt, V.; Miró, E. Novel Ni-Ce-Zr/Al<sub>2</sub>O<sub>3</sub> Cellular Structure for the Oxidative Dehydrogenation of Ethane. *Catalysts* **2017**, *7*, 331. [[CrossRef](#)]
7. Mukherjee, D.; Park, S.E.; Reddy, B.M. CO<sub>2</sub> as a soft oxidant for oxidative dehydrogenation reaction: An eco benign process for industry. *J. CO<sub>2</sub> Util.* **2016**, *16*, 301–312. [[CrossRef](#)]
8. Azzolina-Jury, F.; Bento, D.; Henriques, C.; Thibault-Starzyk, F. Chemical engineering aspects of plasma-assisted CO<sub>2</sub> hydrogenation over nickel zeolites under partial vacuum. *J. CO<sub>2</sub> Util.* **2017**, *22*, 97–109. [[CrossRef](#)]
9. Beran, S. Model calculations of the electrostatic field in ZSM-5 zeolites and its effect on molecules. *J. Mol. Catal.* **1988**, *45*, 225–233. [[CrossRef](#)]
10. He, N.; Xie, H.B.; Ding, Y.H. A theoretical study on the adsorption of an all-metal aromatic molecule Na<sub>2</sub>Al<sub>4</sub> on MCM-22 zeolite. *Microporous Mesoporous Mater.* **2010**, *130*, 67–75. [[CrossRef](#)]
11. Rajadurai, S.; Selvanathan, A.; Mary Selvi, V. Effect of Be<sup>2+</sup> and Ni<sup>2+</sup> Ion substitution on acidity and catalytic activity of A-Type Zeolites. *Mater. Chem. Phys.* **1985**, *12*, 483–489. [[CrossRef](#)]
12. Bae, D.; Park, H.; Seog Kim, J.; Lee, J.B.; Kwon, O.Y.; Kim, K.Y.; Song, M.K.; No, K.T. Hydrogen adsorption in organic ion-exchanged zeolites. *J. Phys. Chem. Solids* **2008**, *69*, 1152–1154. [[CrossRef](#)]
13. Ogo, S.; Sekine, Y. Catalytic Reaction Assisted by Plasma or Electric Field. *Chem. Rec.* **2017**, *17*, 1–14. [[CrossRef](#)] [[PubMed](#)]
14. Deren, J.; Mania, R. Effect of an external electric field on the oxidation of CO to CO<sub>2</sub> on a nickel oxide catalyst. *J. Catal.* **1974**, *35*, 369–375. [[CrossRef](#)]
15. Andres, J.L.; Lled, A.; Duran, M.; Bertran, J. Electric fields acting as catalysts in chemical reactions. An ab initio study of the walden inversion reaction. *Chem. Phys. Lett.* **1988**, *153*, 82–86. [[CrossRef](#)]
16. Sekine, Y.; Tomioka, M.; Matsukata, M.; Kikuchi, E. Catalytic degradation of ethanol in an electric field. *Catal. Today* **2009**, *146*, 183–187. [[CrossRef](#)]
17. Sekine, Y.; Haraguchi, M.; Tomioka, M.; Matsukata, M.; Kikuchi, E. Low-Temperature Hydrogen Production by Highly Efficient Catalytic System Assisted by an Electric Field. *J. Phys. Chem. A* **2010**, *114*, 3824–3833. [[CrossRef](#)] [[PubMed](#)]
18. Sekine, Y.; Haraguchi, M.; Matsukata, M.; Kikuchi, E. Low temperature steam reforming of methane over metal catalyst supported on Ce<sub>x</sub>Zr<sub>1-x</sub>O<sub>2</sub> in an electric field. *Catal. Today* **2011**, *171*, 116–125. [[CrossRef](#)]
19. Tanaka, K.; Sekine, Y.; Oshima, K.; Tanaka, Y.; Matsukata, M.; Kikuchi, E. Catalytic Oxidative Coupling of Methane Assisted by Electric Power over a Semiconductor Catalyst. *Chem. Lett.* **2012**, *41*, 351–353. [[CrossRef](#)]
20. Oshima, K.; Shinagawa, T.; Haraguchi, M.; Sekine, Y. Low temperature hydrogen production by catalytic steam reforming of methane in an electric field. *Int. J. Hydrog. Energy* **2013**, *38*, 3003–3011. [[CrossRef](#)]
21. Oshima, K.; Tanaka, K.; Yabe, T.; Kikuchi, E.; Sekine, Y. Oxidative coupling of methane using carbon dioxide in an electric field over La-ZrO<sub>2</sub> catalyst at low external temperature. *Fuel* **2013**, *107*, 879–881. [[CrossRef](#)]
22. Oshima, K.; Shinagawa, T.; Nogami, Y.; Manabe, R.; Ogo, S.; Sekine, Y. Low temperature catalytic reverse water gas shift reaction assisted by an electric field. *Catal. Today* **2014**, *232*, 27–32. [[CrossRef](#)]
23. Sekine, Y.; Yamagishi, K.; Nogami, Y.; Manabe, R.; Oshima, K.; Ogo, S. Low Temperature Catalytic Water Gas Shift in an Electric Field. *Catal. Lett.* **2016**, *146*, 1423–1428. [[CrossRef](#)]

24. Yabe, T.; Mitarai, K.; Oshima, K.; Ogo, S.; Sekine, Y. Low-temperature dry reforming of methane to produce syngas in an electric field over La-doped Ni/ZrO<sub>2</sub> catalysts. *Fuel Process. Technol.* **2017**, *158*, 96–103. [[CrossRef](#)]
25. Yabe, T.; Kamite, Y.; Sugiura, K.; Ogo, S.; Sekine, Y. Low-temperature oxidative coupling of methane in an electric field using carbon dioxide over Ca-doped LaAlO<sub>3</sub> perovskite oxide catalysts. *J. CO<sub>2</sub> Util.* **2017**, *20*, 156–162. [[CrossRef](#)]
26. Okada, S.; Manabe, R.; Inagaki, R.; Ogo, S.; Sekine, Y. Methane dissociative adsorption in catalytic steam reforming of methane over Pd/CeO<sub>2</sub> in an electric field. *Catal. Today* **2018**, *307*, 272–276. [[CrossRef](#)]
27. Ogo, S.; Iwasaki, K.; Sugiura, K.; Sato, A.; Yabe, T.; Sekine, Y. Catalytic oxidative conversion of methane and ethane over polyoxometalate-derived catalysts in electric field at low temperature. *Catal. Today* **2018**, *299*, 80–85. [[CrossRef](#)]
28. Alamdari, A.; Karimzadeh, R. Faradaic number as a criterion for the promotion effect of external electric field on the heterogeneous oxidative cracking of liquefied petroleum gas on ZSM-5 supported catalyst. *React. Kinet. Mech. Catal.* **2018**, *123*, 723–742. [[CrossRef](#)]
29. Peiqing, Z.; Xiangsheng, W.; Xinwen, G.; Hongchen, G.; Leping, Z.; Yongkang, H. Characterization of Modified Nanoscale ZSM-5 Zeolite and Its Application in the Olefins Reduction in FCC Gasoline. *Catal. Lett.* **2004**, *92*, 63–68. [[CrossRef](#)]
30. Jiang, Y.J.; Juan, J.C.; Meng, X.J.; Cao, W.L.; Yarmo, M.A.; Zhang, J.C. Preparation and Catalytic Application of Novel Water Tolerant Solid Acid Catalysts of Zirconium Sulfate/HZSM-5. *Chem. Res. Chin. Univ.* **2007**, *23*, 349–354. [[CrossRef](#)]
31. Navlani-García, M.; Puértolas, B.; Lozano-Castelló, D.; Cazorla-Amorós, D.; Navarro, M.V. CuH-ZSM-5 as Hydrocarbon Trap under Cold Start Conditions. *Environ. Sci. Technol.* **2013**, *47*, 5851–5857. [[CrossRef](#)] [[PubMed](#)]
32. Liu, J.; La Hong, A.S.N.; He, N.; Liu, G.; Liang, C.; Zhang, X.; Guo, H. The crucial role of reaction pressure in the reaction paths for i-butane conversion over Zn/HZSM-5. *Chem. Eng. J.* **2013**, *218*, 1–8. [[CrossRef](#)]
33. Lu, J.; Liu, Y.; Li, N. Fe-modified HZSM-5 catalysts for ethanol conversion into light olefins. *J. Nat. Gas Chem.* **2011**, *20*, 423–427. [[CrossRef](#)]
34. Vafi, L.; Karimzadeh, R. Effect of phosphorus on methane production in LPG catalytic cracking over modified structure ZSM-5. *J. Nat. Gas Sci. Eng.* **2015**, *27*, 751–756. [[CrossRef](#)]
35. Sang, S.; Chang, F.; Liu, Z.; He, C.; He, Y.; Xu, L. Difference of ZSM-5 zeolites synthesized with various templates. *Catal. Today* **2004**, *93*, 729–734. [[CrossRef](#)]
36. Damjanović, L.; Auroux, A. Determination of Acid/Base Properties by Temperature Programmed Desorption (TPD) and Adsorption Calorimetry. In *Zeolite Characterization and Catalysis*; Chester, A.W., Derouane, E.G., Eds.; Springer: Dordrecht, The Netherlands, 2009; pp. 107–167.
37. López-Fonseca, R.; Gutiérrez-Ortiz, J.I.; Gutiérrez-Ortiz, M.A.; González-Velasco, J.R. Catalytic combustion of chlorinated ethylenes over H-zeolites. *J. Chem. Technol. Biotechnol.* **2003**, *78*, 15–22. [[CrossRef](#)]
38. Rodríguez-González, L.; Hermes, F.; Bertmer, M.; Rodríguez-Castellón, E.; Jiménez-López, A.; Simon, U. The acid properties of H-ZSM-5 as studied by NH<sub>3</sub>-TPD and 27Al-MAS-NMR spectroscopy. *Appl. Catal. A Gen.* **2007**, *328*, 174–182. [[CrossRef](#)]
39. Franke, M.E.; Simon, U. Proton mobility in H-ZSM5 studied by impedance spectroscopy. *Solid State Ion.* **1999**, *118*, 311–316. [[CrossRef](#)]
40. Niwa, M.; Katada, N. Measurements of acidic property of zeolites by temperature programmed desorption of ammonia. *Catal. Surv. Jpn.* **1997**, *1*, 215–226. [[CrossRef](#)]
41. Zakaria, Z.Y.; Linnekoski, J.; Amin, N.A.S. Catalyst screening for conversion of glycerol to light olefins. *Chem. Eng. J.* **2012**, *207–208*, 803–813. [[CrossRef](#)]
42. Van der Borgh, K.; Galvita, V.V.; Marin, G.B. Ethanol to higher hydrocarbons over Ni, Ga, Fe-modified ZSM-5: Effect of metal content. *Appl. Catal. A Gen.* **2015**, *492*, 117–126. [[CrossRef](#)]
43. Biscardi, J.A.; Meitzner, G.D.; Iglesia, E. Structure and Density of Active Zn Species in Zn/H-ZSM5 Propane Aromatization Catalysts. *J. Catal.* **1998**, *179*, 192–202. [[CrossRef](#)]
44. Ralls, K.M.; Courtney, T.H.; Wulff, J. *An Introduction to Materials Science and Engineering*, 1st ed.; John Wiley and Sons: New York, NY, USA, 1976.
45. Izci, E.; Izci, A. Dielectric Behavior of the Catalyst Zeolite NaY. *Turk. J. Chem.* **2007**, *31*, 523–530.
46. Chandrashekhar, G.V.; Cooper, E.; Shafer, M.W. Dielectric Properties of Macro-Defect-Free (MDF) Cements. *Mater. Sci.* **1989**, *24*, 3356–3360. [[CrossRef](#)]

47. Franke, M.E.; Simon, U. Solvate-Supported Proton Transport in Zeolites. *Chem. Phys. Chem.* **2004**, *5*, 465–472. [[CrossRef](#)] [[PubMed](#)]
48. Wang, Y.; Zhu, J.H.; Cao, J.M.; Chun, Y.; Xu, Q.H. Basic catalytic behavior of MgO directly dispersed on zeolites by microwave irradiation. *Microporous Mesoporous Mater.* **1998**, *26*, 175–184. [[CrossRef](#)]
49. Krylov, V. *Catalysis by Non-Metals*; Academic Press: New York, NY, USA, 1970.
50. Morris, B.A. Dielectric study of the synthetic linde type-A zeolite-II. Dielectric properties of 5-A with adsorbed ammonia, sulphur dioxide, carbon dioxide and N-pentane. *J. Phys. Chem. Solids* **1969**, *30*, 89–101. [[CrossRef](#)]
51. Rostovshchikova, T.N.; Smirnov, V.V.; Gurevich, S.A.; Kozhevin, V.M.; Yavsin, D.A.; Nevskaya, S.M.; Nikolaev, S.A.; Lokteva, E.S. Nanostructured metal films: Fabrication and catalytic properties. *Catal. Today* **2005**, *105*, 344–349. [[CrossRef](#)]
52. Borchert, H.; Baerns, M. The Effect of Oxygen-Anion Conductivity of Metal–Oxide Doped Lanthanum Oxide Catalysts on Hydrocarbon Selectivity in the Oxidative Coupling of Methane. *J. Catal.* **1997**, *168*, 315–320. [[CrossRef](#)]
53. Voskresenskaya, E.N.; Roguleva, V.G.; Anshits, A.G. Oxidant Activation over Structural Defects of Oxide Catalysts in Oxidative Methane Coupling. *Catal. Rev. Sci. Eng.* **1995**, *7*, 101–143. [[CrossRef](#)]
54. Grasselli, R.K. Fundamental principles of selective heterogeneous oxidation catalysis. *Top. Catal.* **2000**, *21*, 79–88. [[CrossRef](#)]
55. Jibril, B.Y. Catalytic performances and correlations with metal oxide band gaps of metal-tungsten mixed oxide catalysts in propane oxydehydrogenation. *React. Kinet. Catal. Lett.* **2005**, *86*, 171–177. [[CrossRef](#)]
56. Pantazidis, A.; Bucholz, S.A.; Zanthoff, H.W.; Schuurman, Y.; Mirodatos, C.A. TAP reactor investigation of the oxidative dehydrogenation of propane over a V–Mg–O catalyst. *Catal. Today* **1998**, *40*, 207–214. [[CrossRef](#)]
57. Abbasizadeh, S.; Karimzadeh, R. Effect of Next-Nearest-Neighbor Aluminum Atoms in the HZSM-5 Framework Synthesized with Various Aluminum Sources on Liquefied Petroleum Gas Transformation to Light Olefins. *Ind. Eng. Chem. Res.* **2018**, *57*, 7783–7794. [[CrossRef](#)]
58. Abbasizadeh, S.; Karimzadeh, R. Effect of framework single and close (pairs and un-pairs) aluminum atoms on phosphorous modification of HZSM-5 in cracking of liquefied petroleum gas to ethylene and propylene. *Microporous Mesoporous Mater.* **2018**, *266*, 132–140. [[CrossRef](#)]
59. Arce-Sarria, A.; Machuca-Martínez, F.; Bustillo-Lecompte, C.; Hernández-Ramírez, A.; Colina-Márquez, J. Degradation and Loss of Antibacterial Activity of Commercial Amoxicillin with TiO<sub>2</sub>/WO<sub>3</sub>-Assisted Solar Photocatalysis. *Catalysts* **2018**, *8*, 222. [[CrossRef](#)]
60. Azároff, L.V.; Brophy, J.J. *Electronic Processes in Materials*, 1st ed.; Technology & Engineering; McGraw-Hill: New York, NY, USA, 1963.
61. Banik, A.; Biswas, K. AgI alloying in SnTe boosts the thermoelectric performance via simultaneous valence band convergence and carrier concentration optimization. *J. Solid State Chem.* **2016**, *242*, 43–49. [[CrossRef](#)]
62. El-Hadi, M.A.; Saqan, S.; Zihlif, A.; Ragosa, G. Electrical impedance properties of zeolite composites. *Mater. Technol.* **2008**, *23*, 152–157. [[CrossRef](#)]



© 2018 by the authors. Licensee MDPI, Basel, Switzerland. This article is an open access article distributed under the terms and conditions of the Creative Commons Attribution (CC BY) license (<http://creativecommons.org/licenses/by/4.0/>).